Extratropical Cyclogenesis Changes in Connection with Tropospheric ENSO Teleconnections to the North Atlantic: Role of Stationary and Transient Waves

SEBASTIAN SCHEMM

Geophysical Institute, University of Bergen, and Bjerknes Centre for Climate Research, Bergen, Norway, and Institute for Atmospheric and Climate Science, ETH Zürich, Zürich, Switzerland

GWENDAL RIVIÈRE

LMD/IPSL, École Normale Supérieure, and PSL Research University, Sorbonne Université, and École Polytechnique, CNRS, Paris, France

LAURA M. CIASTO

NOAA/NWS/NCEP/Climate Prediction Center, and Innovim, LLC, Greenbelt, Maryland

CAMILLE LI

Geophysical Institute, University of Bergen, and Bjerknes Centre for Climate Research, Bergen, Norway

(Manuscript received 14 November 2017, in final form 19 July 2018)

ABSTRACT

This study investigates mechanisms for changes in wintertime extratropical cyclogenesis over North America and the North Atlantic during different phases of El Niño–Southern Oscillation (ENSO). Insights into the relationship between the ENSO–North Atlantic teleconnection and the cyclogenesis changes are provided by diagnosing the relative roles of stationary wave propagation and transient eddies in setting cyclogenesis-conducive large-scale circulation anomalies. During La Niña winters, Rocky Mountain and Greenland cyclogenesis are enhanced, while Gulf Stream cyclogenesis is reduced. Diagnostics suggest that stationary waves of tropical origin work in tandem with transient eddies to amplify the ridge over the northeastern Pacific, establishing background flow anomalies that favor Rocky Mountain cyclogenesis; downstream, more transient eddies with an anticyclonic tilt push the North Atlantic jet poleward, favoring cyclogenesis near Greenland, while contributions from stationary waves are small. During central Pacific El Niño winters, the cyclogenesis situation is essentially the opposite: Rocky Mountain and Greenland cyclogenesis are reduced, while Gulf Stream cyclogenesis is enhanced. The analyses are consistent with stationary waves and transient eddies acting to weaken the climatological ridge over the northeastern Pacific, creating a more zonal Pacific jet; downstream, transient eddies with a cyclonic tilt push the North Atlantic jet equatorward, favoring Gulf Stream cyclogenesis. Anomalies in cyclogenesis frequencies, and the relative roles of transient and stationary waves, during eastern Pacific El Niño winters are associated with larger uncertainties.

1. Introduction

Tropical Pacific sea surface temperatures (SSTs) influence midlatitude atmospheric variability through hemispheric-spanning teleconnection patterns [Exner 1914; Horel and Wallace 1981; Hurrell 1996; Trenberth et al. 1998; Trenberth and Caron 2000; Alexander et al. 2002; Ciasto and Thompson 2008; Frauen et al. 2014; Deser et al. 2017; and see extended reviews in Hoerling and Kumar (2002) and Stan et al. (2017)]. The dominant

Denotes content that is immediately available upon publication as open access.

Corresponding author: Sebastian Schemm, sebastian.schemm@env.ethz.ch

DOI: 10.1175/JAS-D-17-0340.1

mode of tropical Pacific SST variability, El Niño–Southern Oscillation (ENSO), affects weather and climate over much of the globe even in high-latitude regions with potential impacts on surface temperature trends over Greenland (Ding et al. 2014), Arctic sea ice variability (Wettstein and Deser 2014; Ding et al. 2017), and heat transport into polar regions (Park et al. 2015). In the North Atlantic–European sector, however, determining the robust signals of ENSO has been a challenge (Brönnimann et al. 2007). During El Niño winters, there is a tendency for negative North Atlantic Oscillation (NAO)-like conditions (i.e., equatorward-shifted North Atlantic jet, lower than normal temperatures over northern Europe; increased precipitation over southern Europe), and vice versa during La Niña (van Loon and Madden 1981; May and Bengtsson 1998; Moron and Plaut 2003; Brönnimann et al. 2007; García-Serrano et al. 2011; Li and Lau 2012a; Rodríguez-Fonseca et al. 2016) although there is some debate over whether ENSO truly triggers the NAO (García-Serrano et al. 2011).

A classical view on how these teleconnection signals are transmitted is via stationary Rossby wave propagation that alters the time-mean extratropical flow (Hoskins and Karoly 1981; Hoskins and Ambrizzi 1993; Honda et al. 2001; Held et al. 2002; Moron and Gouirand 2003). The Rossby waves follow great-circle pathways from the tropics into the midlatitudes (Hoskins and Karoly 1981; Hoskins and Ambrizzi 1993), along ray paths that depend on the midlatitude flow (Branstator 1985). In this way, tropical Pacific SST variability is assumed to drive changes in midlatitude storm tracks (e.g., May and Bengtsson 1998; Moron and Plaut 2003; Eichler and Higgins 2006; Ciasto et al. 2016; Branstator 2014) and consequently regional climate, for example, seasonally averaged precipitation and surface temperatures over North America (e.g., Ropelewski and Halpert 1987; Halpert and Ropelewski 1992; Gershunov and Barnett 1998; Seager et al. 2010; Smith and Sardeshmukh 2000; Yu et al. 2012).

This classical view on the way ENSO teleconnections are transmitted has been gradually augmented by new insights into how transient eddies help to shape the observed midlatitude circulation response, in particular over the North Atlantic. This extension of the classical stationary wave perspective assumes that the extratropical circulation response to tropical variability arises from an interplay between the stationary large-scale flow changes and transient extratropical eddy activity, rather than from the first alone (May and Bengtsson 1998; Moron and Plaut 2003; Pozo-Vázquez et al. 2005; Toniazzo and Scaife 2006; Li and Lau 2012b,a; Drouard et al. 2015). This combined interaction produces what is commonly referred to as ENSO's tropospheric pathway into the North Atlantic. The general idea is no surprise. Held et al. (1989) used a linearized stationary wave model to argue that the extratropical wave trains simulated by a GCM forced by anomalous tropical heating combine a direct effect of the heating and a modulating effect of the anomalous transients (Held et al. 1989). This is also true for relatively short-lived tropical heating events in idealized atmospheric GCM experiments (Branstator 2014).

The important role of transient upper-level eddies (i.e., troughs and ridges) in shaping the North Atlantic circulation response during ENSO-affected winters was recently solidified by studies relying on reanalysis data. In late winter (January–March), for example, it matters how exactly transient upper-level eddies form and propagate downstream from North America (Li and Lau 2012b,a). During La Niña winters, an amplified stationary ridge over the northeastern Pacific is associated with transient eddies that tend to have a more equatorward orientation, favoring anticyclonic wave breaking over the North Atlantic and pushing the North Atlantic jet poleward (positive NAO-like); the opposite occurs during El Niño winters to produce a negative NAO-like response (Li and Lau 2012b,a; Drouard et al. 2015). The described mechanism has been confirmed using quasigeostrophic modeling experiments (Drouard et al. 2013). A preliminary first link between the different downstream propagating upper-level transient eddies and the North Atlantic surface storm track is provided by Schemm et al. (2016), who showed a preference for Gulf Stream cyclogenesis to occur below the North Atlantic jet exit rather than in the climatologically preferred location below the jet entrance. Consequently, this study is motivated to extend the results of Schemm et al. (2016) by

- investigating changes in all cyclogenesis regions that feed into the North Atlantic storm track during all phases of ENSO,
- identifying the large-scale dynamics associated with the differences, and
- linking differences in the large-scale flow to the earlier findings on upper-level transient eddies and stationary wave propagation.

For completeness, we note that there is an alternative pathway for ENSO teleconnections to the North Atlantic. It is proposed to work via a response in the stratospheric circulation to ENSO (Brönnimann et al. 2004; Manzini et al. 2006; Garfinkel and Hartmann 2008; Ineson and Scaife 2009; Butler et al. 2014; Domeisen et al. 2015), and a subsequent downward propagation of temperature anomalies (Plumb and Semeniuk 2003; Hardiman and Haynes 2008; Ineson and Scaife 2009; Polvani et al. 2017). Research on this "stratospheric

ENSO pathway'' is vital but complicated by the fact that it seems to be nonstationary, dependent on multidecadal variability (Greatbatch et al. 2004; Toniazzo and Scaife 2006; Garfinkel and Hartmann 2008; Zanchettin et al. 2008; Richter et al. 2015; López-Parages et al. 2016), and possibly affected by tropospheric and event-to-event ENSO variability (Garfinkel and Hartmann 2008; Garfinkel et al. 2012, 2013a,b). Further, the mutual interaction between the stratospheric and the tropospheric pathways is still under investigation (Butler et al. 2014; Jiménez-Esteve and Domeisen 2018).

The study is organized as follows. Data and methods are presented in section 2. In section 3, we explore the cyclogenesis regions relevant for the North Atlantic storm track, including their climatology and associated large-scale upper-level dynamics. In section 4, we examine extratropical cyclogenesis frequency and related large-scale dynamics during different ENSO phases and how they differ relative to the climatological mean discussed in section 3. In section 5 we study the role of stationary and transient waves for creating the background flow anomalies that are associated with variability in extratropical cyclogenesis during ENSO. A summary is presented in section 6.

2. Data and methods

a. Surface cyclone and cyclogenesis detection

The detection of surface cyclones and cyclogenesis is based on the method introduced by Wernli and Schwierz (2006). The scheme identifies closed contours in sea level pressure (SLP) and tracks them in 6-hourly ERA-Interim data (1979–2015) during December–February. A track is accepted if the minimum lifetime exceeds 24 h. The point of cyclogenesis is defined as the location of the minimum SLP inside a closed SLP contour at the first time step of a surface cyclone track. Further refinements introduced to the original scheme include the treatment of splitting and merging events, as described in Sprenger et al. (2017). These refinements do not affect the results of this study.

b. Lagrangian parcel trajectories and probability density

The computation of Lagrangian parcel trajectories and probability densities of trajectories follows Schemm et al. (2016). Trajectory calculations are performed using the Lagrangian Analysis Tool (LAGRANTO) of Sprenger and Wernli (2015). For every cyclogenesis event, trajectories are calculated backward starting at each grid point within a 500-km radius centered on the location of cyclogenesis. In the vertical, the starting positions are staggered by increments of 5 hPa in the 400–200-hPa layer. To obtain a smooth, gridded position density field from the bundle of backward calculated trajectories, all grid points within a radius of 300 km around the interpolated position of the individual trajectories are flagged with a value of one to indicate the presence of a trajectory. The resulting sum at every grid point represents the number of trajectories located near this grid point at a certain time step, for example, 48 h before cyclogenesis. The summed field is normalized by the gridpoint area and the total number of trajectories, then by its integral over Earth's surface such that we obtain an air-parcel probability that integrates to unity at each time step.

c. Horizontal wind decomposition

To understand the precyclogenesis dynamics, we adopt a traditional eddy–mean flow perspective to decompose the total horizontal wind field into a transient flow component, computed using a 6-day high-pass filter, and a slowly varying background flow component, computed using a 10-day low-pass filter. A Lanczos filter with 21 weights is applied to 6-hourly ERA-Interim data to obtain high- and low-pass-filtered wind velocities. (The two components do not sum to the total flow field, but the discrepancy is not problematic for the descriptive part of our study.) The frequency-filtered flow fields are computed on 400-, 300-, and 200-hPa levels and averaged in the vertical. To depict anomalies in the background flow component, the long-term (1979–2015) climatological mean is subtracted.

d. ENSO definition

The definitions of El Niño and La Niña seasons are based on the NOAA oceanic Niño index (ONI), which is computed by applying a 3-month running mean of the SST anomaly in the Niño-3.4 region (5°N–5°S, 120°–170°W) with a 30-yr mean removed. Historically, ONI values below/above 0.5 are considered to be affected by ENSO if the threshold is met for a minimum of five consecutive overlapping 3-month seasons (spanning 7 months in total). For the definition of EP and CP El Niño winters (December–February) we use three different methods proposed by Kao and Yu (2009), Yeh et al. (2009), and Ashok et al. (2007) and rely on a consensus (at least two out of three methods agree) as suggested by Yu et al. (2012). This gives four EP El Niño winters (1982/83, 1986/87, 1997/98, and 2006/07); six CP El Niño winters (1987/88, 1991/92, 1994/95, 2002/03, 2004/05, and 2009/10); and five strong La Niña winters (ONI < -1; 1988/89, 1998/99, 1999/2000, 2007/08, and 2010/11). Section 2e describes our approach for significance testing. A consensus between all three methods exists for only three out of six identified CP (i.e., 1994/95, 2004/05, and 2009/10)

and EP (i.e., 1982/83, 1997/98, and 2006/07) El Niño winters. Accordingly, our findings may deviate from the results of previous studies if these are based on a single method. For example, Graf and Zanchettin (2012) classify the winter 1986/87 as CP El Niño, which is in agreement with the method of Kao and Yu (2009). However, the two other methods classify this season as EP El Niño, as do we.

e. Significance

To assess the significance of our cyclogenesis composites, we use random sampling techniques. For example, to test the significance of results that are based on five La Niña winters, we randomly choose with replacement five winter seasons 2000 times from all winters between 1979 and 2015, to produce a randomized distribution of five-winter composites. This distribution is used to assign a p value to every grid point in the La Niña composite, indicating the probability that a similar or more extreme result would be observed by chance (i.e., the null hypothesis is that the result is random noise). Then, we test for global (i.e., field) significance following the approach of Wilks (2016). Local (grid point) null hypotheses are rejected only if their p value is below a global p value defined by $p^* = \max[p_i \leq (i/N)\alpha]$, where N is the total gridpoint number, i is the rank in the sorted distribution of all p values and α a chosen control level that corresponds to the fraction of grid points in the domain that are erroneously rejected (we start with $\alpha = 0.1$). The North American and Atlantic domains over which p^* is computed are shown in the figures.

Further, we use a bootstrapped statistic to determine how sampling variability influences the result that tropical Pacific SST variability changes the odds of a season having higher/lower than normal cyclogenesis counts in the regions of interest. Following Deser et al. (2017), the procedure is based on the assumption that ENSO events are exchangeable (Deser et al. 2017). We compute a large ensemble of randomized synthetic ENSO composites by randomly sampling 10^5 times with replacement, for the period 1979–2015, 11 winters from all 11 winters with a high ($\geq$0.5) ONI index, 11 winters with replacement from all 11 winters with a low (≤ -0.5) ONI index, and 12 winters with replacement from all 12 neutral winters. For each of the 10^5 synthetic composites, each consisting of 11 or 12 randomly selected winters, we compute the mean cyclogenesis number per winter in the region of interest. The three obtained distributions are used to assess whether there is a systematic change in the odds for cyclogenesis over different regions.

f. Wave propagation diagnostics

To diagnose the influence of wave propagation on the low-frequency midlatitude flow, we use the wave activity flux formulation derived by Plumb (1985) for stationary waves, and the **E** vector of Hoskins et al. (1983) and Trenberth (1986) for transient waves.

1) Stationary wave propagation

The wave activity flux formulation derived by Plumb (1985) is well suited to depict large-scale stationary wave propagation on a steady mean flow. In the examples presented in Plumb (1985) and Karoly et al. (1989), the wave activity flux is used to identify diabatic processes, jet instabilities, and orography as the primary sources of climatological Rossby wave trains in the midlatitudes. In another example presented by Ding et al. (2014), the wave activity flux is applied to identify the tropical forcing of the recent warming over Greenland. We restrict our analysis to the horizontal components of the wave activity flux formulated in pressure coordinates:

$$\mathbf{F}_s = p\cos(\phi)\left\{\begin{array}{l} \dfrac{1}{2a^2\cos^2(\phi)}\left[\left(\dfrac{\partial\psi'}{\partial\lambda}\right)^2 - \psi'\dfrac{\partial^2\psi'}{\partial\lambda^2}\right] \\ \dfrac{1}{2a^2\cos(\phi)}\left(\dfrac{\partial\psi'}{\partial\lambda}\dfrac{\partial\psi'}{\partial\phi} - \psi'\dfrac{\partial^2\psi'}{\partial\lambda\,\partial\phi}\right) \end{array}\right\}, \quad (1)$$

where p denotes the pressure divided by 1000 hPa, a is the radius of Earth, and ψ' is the stationary streamfunction anomaly. The first term in each component represents the eddy transport of meridional and zonal momentum, respectively. The second terms relates to the convergence of eddy-induced ageostrophic geopotential flux [see also Eq. (7.1) in Plumb (1985)]. The conventional procedure to obtain the anomalous stationary streamfunction is to remove the zonal mean from a time-averaged flow field. For anomalies associated with ENSO winters, an extra step is required. First we time average the low-frequency flow over all El Niño or La Niña winters and subtract the long-term winter climatological mean before removing the zonal mean to obtain the stationary streamfunction anomalies. The wave activity flux is generally interpreted as the contribution by stationary Rossby waves to the formation of stationary asymmetries in the time-mean zonal flow. More detailed examples for interpreting this diagnostic are presented in Karoly et al. (1989) and Nakamura et al. (1997). For example, Nakamura et al. (1997) show that during the growing phase of a blocking event, wave activity is typically absorbed prior to Rossby wave breaking, while during the breakdown of a blocking event, wave activity is emitted.

2) Transient wave propagation

To analyze the transient eddy mean–flow interaction, we employ the **E** vector formulation of

Hoskins et al. (1983) in the version presented in Trenberth (1986). The **E** vector is defined as

$$\mathbf{E} = \begin{bmatrix} \frac{1}{2}(\overline{v^{*2} - u^{*2}}) \\ -\overline{u^* v^*} \end{bmatrix}, \qquad (2)$$

where the overbar indicates a time average, and the asterisk indicates a deviation from the time average. We use the high-frequency-filtered flow component (6-day cutoff) to obtain the transient zonal (u^*) and meridional (v^*) flow anomalies at 6-hourly time steps before time averaging the vector components over all El Niño and La Niño seasons. The **E** vector divergence (convergence) suggests regions of eddy-induced acceleration (deceleration) of the zonal mean flow (Hoskins et al. 1983). The **E** vector orientation represents the horizontal eddy orientation: equatorward-pointing **E** vectors indicate southwest–northeast-oriented eddies, which corresponds to a more anticyclonic tilt, while poleward-pointing **E** vectors indicate southeast–northwest-oriented eddies, or a cyclonic tilt (Hoskins et al. 1983; Rivière et al. 2003; Drouard et al. 2015). For meridionally (zonally) elongated eddies, the **E** vector points eastward (westward).

3. Extratropical cyclogenesis and related background flow anomalies in the full winter climatology

In this section, we examine the large-scale dynamics preceding cyclone formation in the main cyclogenesis regions for the North Atlantic storm track. This analysis considers the full winter climatology, without yet distinguishing between ENSO phases.

a. *Preferred regions of surface cyclogenesis for the North Atlantic storm track*

Enhanced extratropical cyclogenesis frequency, which is the relative fraction of time steps affected by cyclogenesis, occurs in several preferred regions (Fig. 1): leeward of mountains, for example, east of the Rocky Mountains (labeled 1 and 2); in regions of enhanced baroclinicity, for example, over the Gulf Stream (labeled 3); and southeast of Greenland, which shares both characteristics (labeled 4). Further, cyclogenesis frequencies are enhanced at the end of the North Atlantic storm track (labeled 5), and in the Mediterranean (labeled 6). Downstream development (Simmons and Hoskins 1979; Chang 1993) and cyclone splitting likely contribute to cyclogenesis at the end of the storm track, while frontal wave cyclogenesis (Parker 1998; Schemm and Sprenger 2015) can play an additional role. The findings are qualitatively in good agreement with earlier studies, including studies that relied on different techniques to identify extratropical cyclones (Hoskins and Hodges 2002, their Fig. 5c). Because the cyclogenesis regions west of Norway and over the Mediterranean do not feed into the North Atlantic storm track, these two regions are excluded from the rest of the analyses.

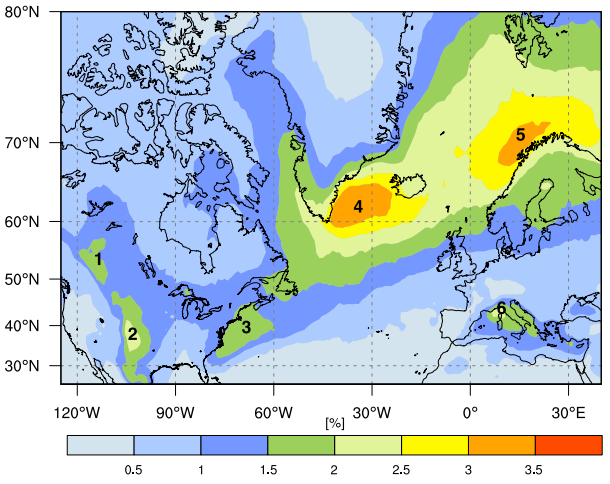

FIG. 1. Cyclogenesis climatology (color; %) for December–February (1979–2015). Frequency indicates the number of time steps affected by a cyclogenesis event.

Extratropical cyclogenesis influences overall cyclone frequencies, but in different ways for different regions (Fig. 2). Cyclones that form in the lee of the Rockies make up approximately 70% of all cyclones over the central United States, decreasing to 10% of all cyclones south of Greenland (Fig. 2a). Cyclone formation over the southern tip of Greenland (Fig. 2b) accounts for up to 40% of the cyclone frequency in the storm track at Greenland. Cyclones with genesis below the North Atlantic jet entrance (southern part of red box in Fig. 2c) account for up to 70% of the total cyclone frequency in the Gulf Stream area. Cyclones forming below the North Atlantic jet exit (northern part of red box in Fig. 2d) account for 30% of all cyclones over the Gulf Stream area. Gulf Stream and Greenland cyclones jointly account for approximately 80% of all cyclones in the North Atlantic storm track.

b. *Precyclogenesis upper-level flow dynamics for Rocky Mountain, Gulf Stream, and Greenland cyclogenesis*

Are there large-scale upper-level circulation anomalies that tend to favor cyclogenesis in the regions of interest? Quasigeostrophic (QG) theory predicts large-scale upward motion east of an upper-level trough caused by forcing by upper-level divergence (Bluestein 1993; Holton 2004). The formation of surface low pressure systems are frequently observed east (ahead) of

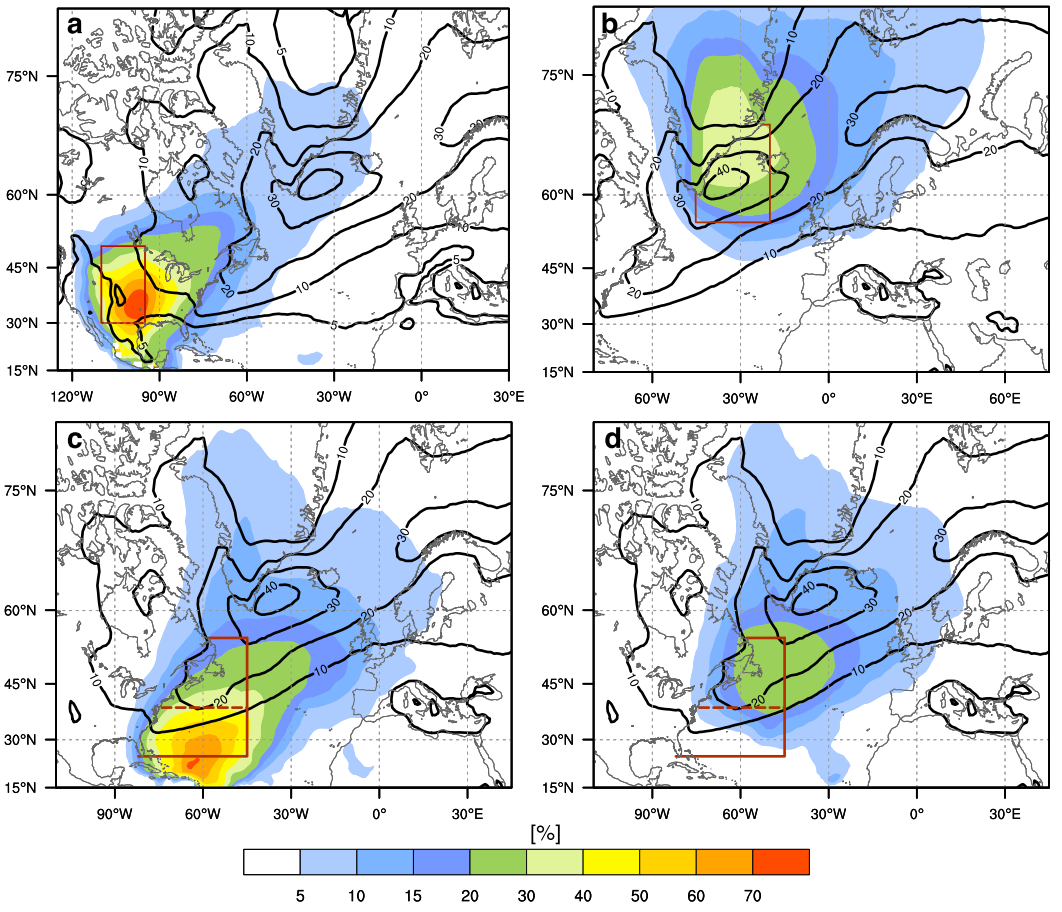

FIG. 2. Relative contributions (color; %) of different cyclogenesis regions to the total cyclone frequency [black contours; 10%, 20%, 30%, and 40%; (a) additionally shows 5%] for cyclogenesis (a) leeward of the Rocky Mountains, (b) at Greenland, and below the North Atlantic jet (c) entrance and (d) exit regions.

troughs, where vertical stretching of the tropospheric air column increases vorticity (Holton 2004). Thus, the presence of an upper-level trough prior to cyclogenesis can be expected, positioned slightly upstream of where the surface pressure low eventually forms.

The following precyclogenesis composites comprise approximately 500 Rocky Mountain cyclogenesis events, 400 Greenland cyclogenesis events, and 350 (450) Gulf Stream exit (entrance) cyclogenesis events. Particular focus is on the background wind (computed using a 10-day low-pass filter), its anomalies with respect to the climatological mean, and transient waves (computed using a 6-day high-pass filter).

1) ROCKY MOUNTAIN CYCLOGENESIS

At 72 h before Rocky Mountain cyclogenesis, the background wind exhibits anomalies (black contour in Fig. 3g) relative to the climatological mean (green contours in Fig. 3g) near the exit region of the Pacific jet. The background winds are enhanced in a band extending from the Bay of Alaska toward western Canada. Two days before Rocky Mountain cyclogenesis, a transient wave train develops in the exit region of the Pacific jet (color shading in Fig. 3e). During the following 24 h, it propagates eastward, confined to the band of anomalously strong background wind. The transient wave amplifies while crossing the Rocky Mountains (Figs. 3a,c). Once the leading edge of the trough anomaly (red shading in Fig. 3a) arrives in the target region, cyclogenesis occurs 6 h later.

The right panels of Fig. 3 illustrate the Lagrangian perspective of the precyclogenesis dynamics, which allows us to identify the source region of cyclogenetic air, air parcels in the upper troposphere above the surface cyclone at genesis. In the case of Rocky Mountain cyclogenesis, the cyclogenetic air originates from the exit region of the Pacific jet (Fig. 3h). Throughout the 72-h precyclogenesis period (Figs. 3b–h), the air advects eastward into the target region [i.e., the cyclogenetic air follows a pathway along the band of enhanced

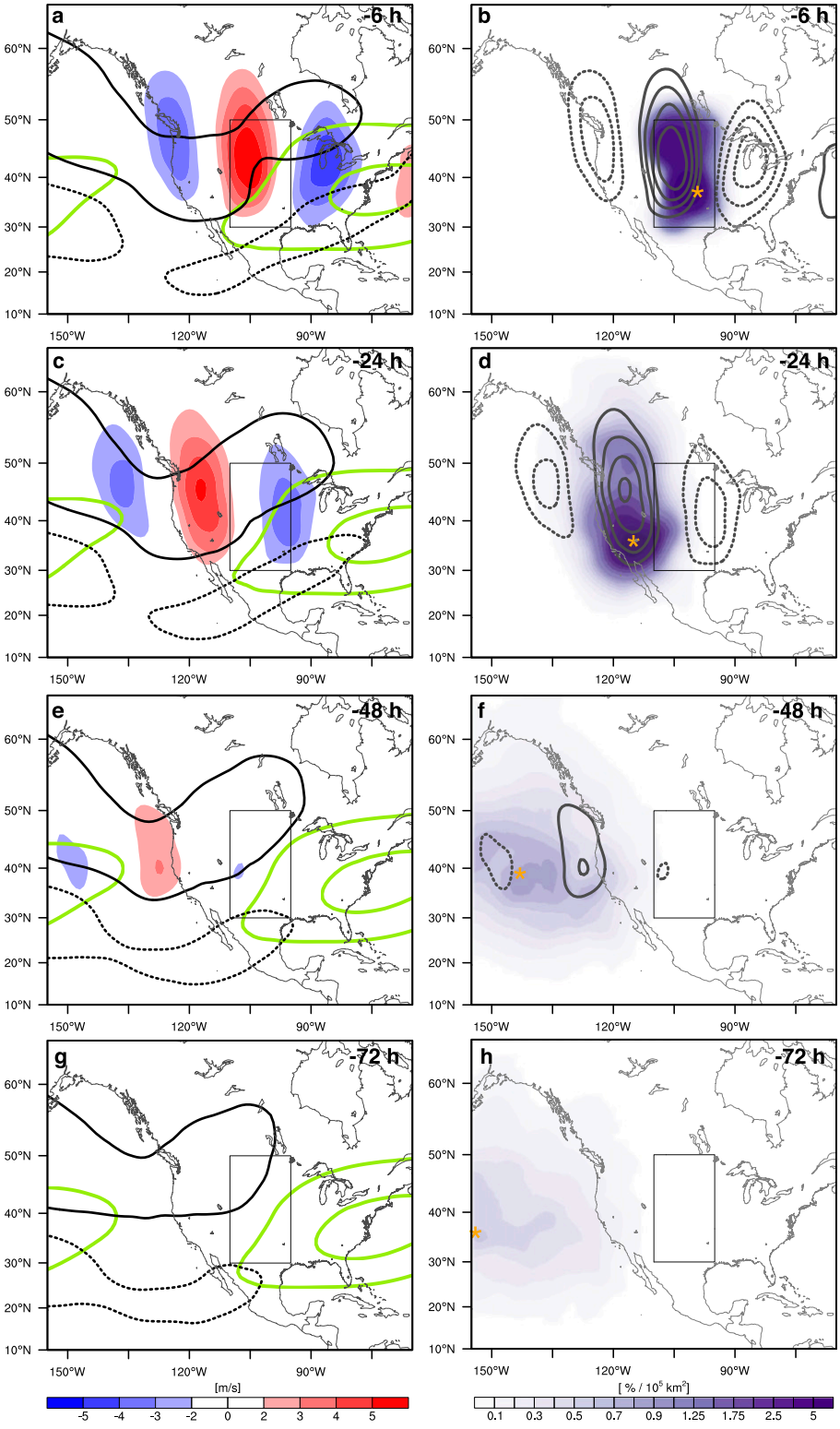

FIG. 3. Rocky Mountain precyclogenesis composites at (a),(b) 6; (c),(d) 24; (e),(f) 48; and (g),(h) 72 h prior to cyclogenesis. (left) High-frequency meridional wind (color; m s^{-1}; 6-day high pass), background wind (green contours; m s^{-1}; 10-day low-pass zonal wind), and background wind anomaly (black contours; negative dashed, positive solid; 1.5 m s^{-1}). All fields are vertically averaged between 400 and 200 hPa. (right) Probability density for air parcels located at cyclogenesis between 400 and 200 hPa (color). Black contours show high-frequency meridional wind. Yellow markers highlight the maximum in the density.

background winds along with the transient wave train (Fig. 3; left column)].

2) GREENLAND CYCLOGENESIS

Greenland cyclogenesis (Fig. 4g) is also preceded by background flow anomalies, in this case, enhanced westerlies across the North Atlantic from Newfoundland toward the United Kingdom (Fig. 4g, solid black contour). Two days before Greenland cyclogenesis, a transient wave develops over the Gulf Stream (Fig. 4g), subsequently amplifies (Figs. 4c–e), and the transient trough anomaly enters the target region 6 h before cyclogenesis (red shading in Fig. 4a), after which a surface cyclone forms.

For Greenland cyclogenesis, the source region of the cyclogenetic air is above Hudson Bay (Fig. 4h). Subsequently, the air advects eastward within the narrow band of enhanced background wind and aligns with the leading edge of the transient trough at Greenland's southern tip 6 h before cyclogenesis (Fig. 4a). We note that while the transient wave develops over the Gulf Stream area, the air constituting the surface cyclone in the upper troposphere has its origin farther poleward over Hudson Bay.

3) GULF STREAM CYCLOGENESIS

Gulf Stream cyclogenesis will be split into two cases: events that occur near the right jet entrance, and events that occur near the left jet exit. Both regions experience large-scale lifting, and hence are favorable for the formation of cyclones.

For Gulf Stream entrance cyclogenesis, it appears that a transient wave train begins developing before any background flow anomaly (Fig. 5g), in contrast to Rocky Mountain or Greenland cyclogenesis. By 24 h before cyclogenesis, both features are well developed (Fig. 5c). The transient trough anomaly arrives in the target region just before cyclogenesis occurs (Fig. 5a). The cyclogenetic air for entrance cyclogenesis comes from Pacific, taking a subtropical path across North America (Figs. 5h,f,d,b) as described in Schemm et al. (2016).

Gulf Stream cyclogenesis below the jet exit is perhaps the most complex case. Three days before cyclogenesis (Fig. 6g), a well-developed transient wave train is already in place over North America. Upstream, two possible pathways for a second wave train are observed (black asterisk in Fig. 6g). During the following 24 h, the leading transient wave train propagates eastward over the North Atlantic. The transient trough anomaly that triggers cyclogenesis (black asterisks in Fig. 6e) approaches the target region from the northwest. The wave train passes by the *left entrance* of the jet, where there is large-scale sinking (rather than lifting) that tends to suppress cyclone formation (Bluestein 1993; Holton 2004). It is only when the transient trough anomaly reaches the left jet exit that cyclogenesis can occur (Fig. 6a). Other factors, such as jet curvature (Clark et al. 2009) or surface fronts (Graf et al. 2017; Schemm et al. 2018), are additional factors that can foster cyclogenesis near the jet exit rather than in the entrance region (Clark et al. 2009).

For Gulf Stream exit cyclogenesis, a broader source region of cyclogenetic air is identified in agreement with the previously described pathways of the transient wave train (Fig. 6h). Upper-level air masses above the surface cyclone at genesis originate off the U.S. West Coast and poleward over northwestern Canada three days beforehand (yellow asterisks in Figs. 6f and 6h). The pathway is shifted poleward relative to the pathway for Gulf Stream entrance cyclogenesis, consistent with previous findings described in Schemm et al. (2016).

4) SUMMARY OF PRECYCLOGENESIS DYNAMICS

In all three examined regions, cyclogenesis is preceded by the formation of an upper-level transient wave train. For the Rocky Mountain and Greenland cases, the wave trains are associated with the presence of preexisting (at least 72 h before cyclogenesis) background flow anomalies; for the Gulf Stream case, the background flow anomalies develop in a relatively shorter time window preceding surface cyclogenesis. The transient trough anomaly is observed to arrive at the target area just before surface cyclogenesis. Vertical lifting ahead of the trough (Bluestein 1993; Holton 2004) promotes cyclogenesis (e.g., Graf et al. 2017), resulting in the formation of a surface cyclone downstream (east) of the upper-level trough. For the case of Gulf Stream cyclogenesis a detailed discussion of the precyclogenesis dynamics in the middle and lower troposphere is provided in Schemm et al. (2016).

Finally, the "significance" of the transient wave trains deserves some comment. Upper-level troughs are highly variable features of wide-ranging size, shape, and orientation. Visual inspection of individual cyclogenesis cases confirms that the precyclogenesis wave trains exhibit substantial diversity. The transient wave train signal emerging in the Rocky Mountain cyclogenesis composite (500 events) is approximately 0.6–0.7 standard deviations of the climatology; for Greenland cyclogenesis (400 events), it is 0.5–0.6 standard deviations; for Gulf Stream entrance cyclogenesis (450 events), it is 0.4–0.5 standard deviations; and for Gulf Stream exit cyclogenesis (350 events), it is 0.1–0.2 standard deviations. Gulf Stream exit cyclogenesis hence exhibits the highest case-to-case variability, resulting in a weak signal relative to the climatological mean. However, because cyclogenesis occurs for

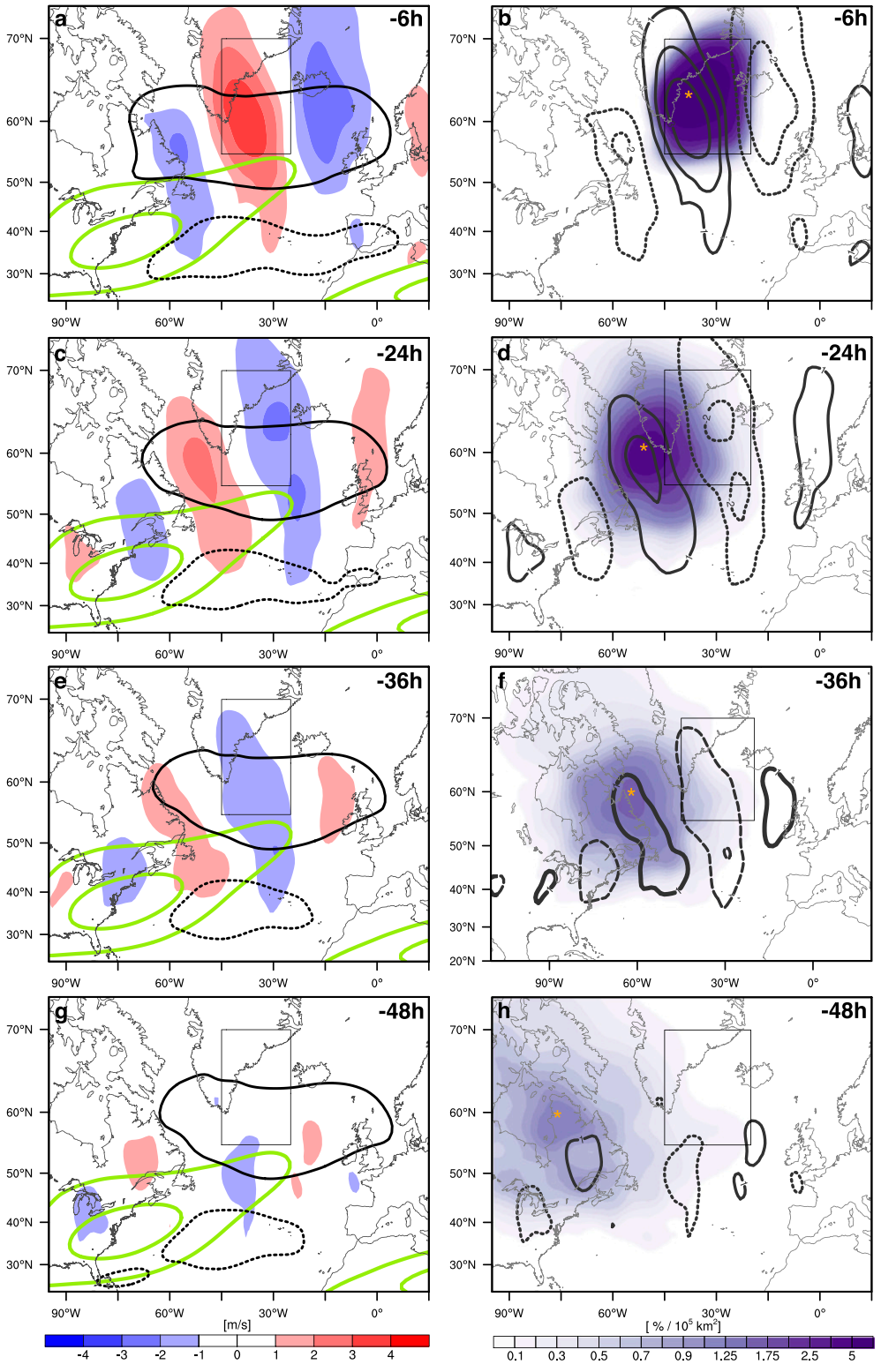

FIG. 4. As in Fig. 3, but for Greenland cyclogenesis (boxed).

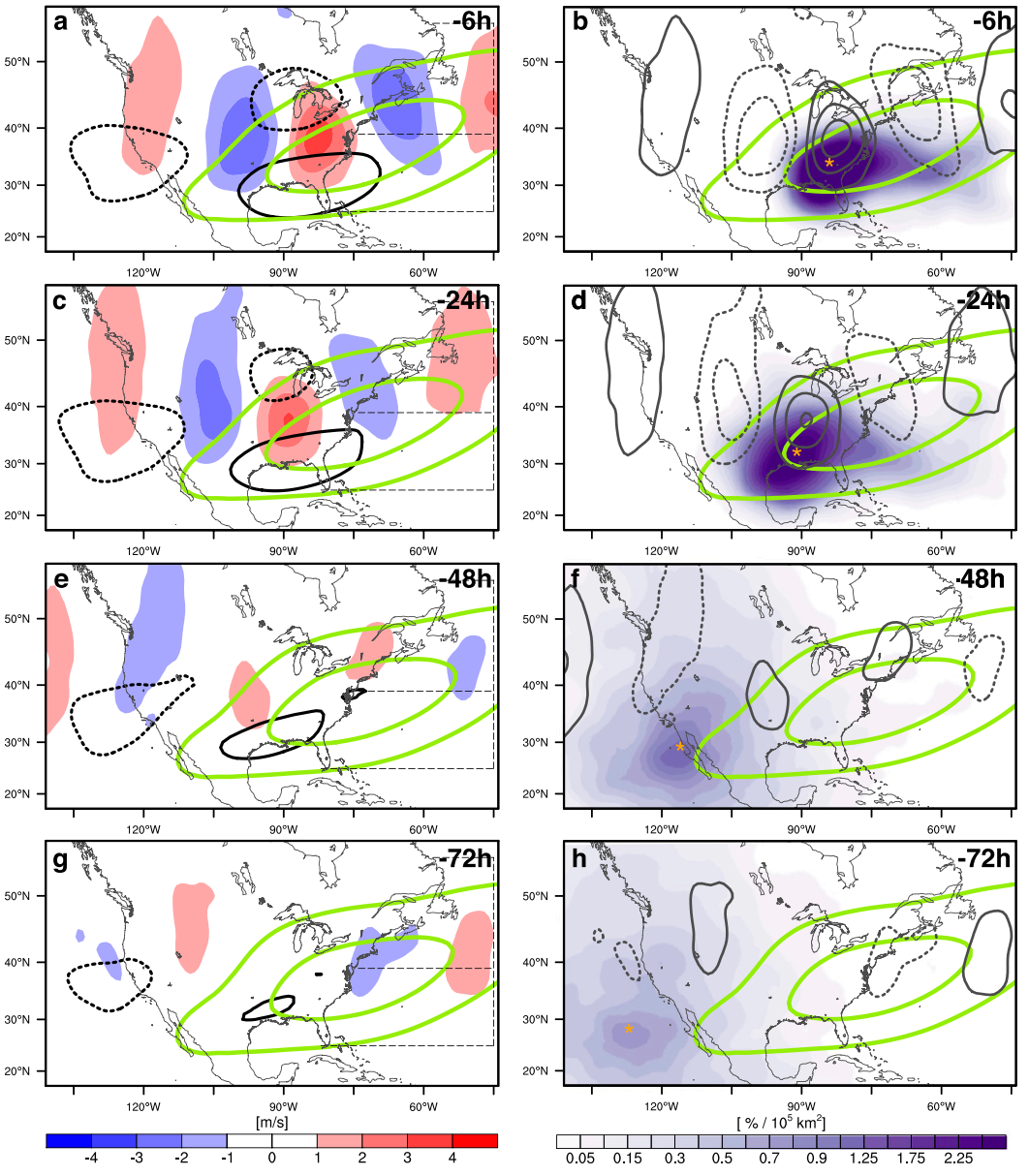

FIG. 5. As in Fig. 3, but for Gulf Stream cyclogenesis below the jet entrance (lower part of dashed box over Gulf Stream region).

all cases, we consider each individual wave train in the composite as physically relevant, despite the high case-to-case variability that results in weak statistical significance.

4. Extratropical surface cyclogenesis and related background flow anomalies during ENSO

Next, we turn our attention to the cyclogenesis anomalies associated with ENSO. It will be shown that the three examined cyclogenesis locations (Rocky Mountains, Greenland, and Gulf Stream regions) exhibit distinct anomalies in cyclogenesis frequency during EP El Niño, CP El Niño, and La Niña winters. Seasonal-mean background flow anomalies associated with the three different ENSO phases resemble the background flow anomalies seen climatologically at cyclogenesis in the three examined regions.

a. Variability in extratropical cyclogenesis for different ENSO phases

During La Niña winters, cyclogenesis frequencies are enhanced leeward of the Rocky Mountains and around the southern tip of Greenland, while they are reduced over the Gulf Stream region (shading in

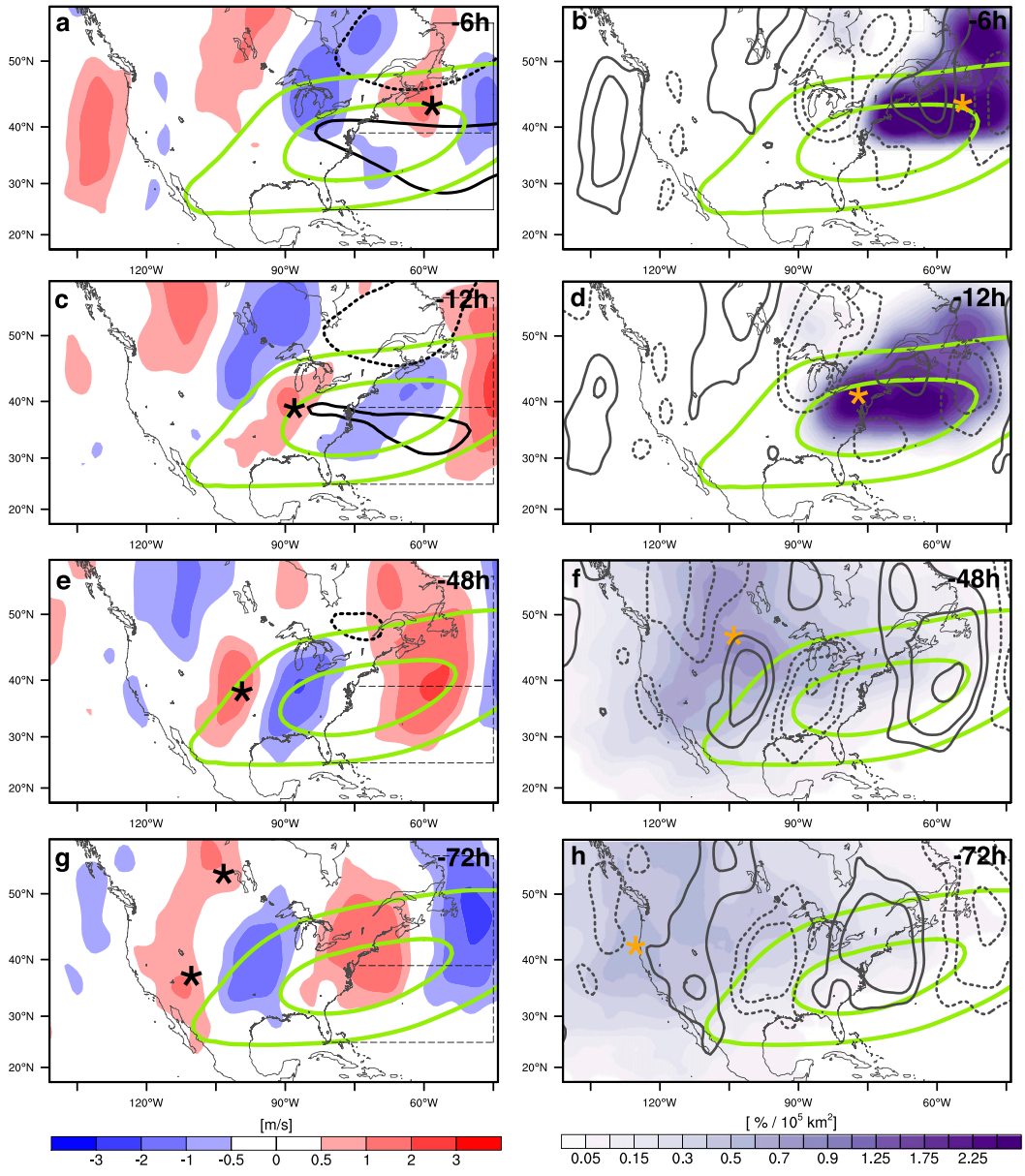

FIG. 6. As in Fig. 3, but for Gulf Stream cyclogenesis below the jet exit (upper part of dashed box over Gulf Stream region). Black marker indicates transient trough anomaly associated with cyclogenesis. Yellow marker indicates the maximum in cyclogenetic air density.

Fig. 7a). These changes in cyclogenesis frequency are associated with clear changes in total cyclone frequency farther downstream (solid contours in Fig. 7a), where we see more cyclones across the Iceland and Nordic seas, and fewer cyclones into the United Kingdom and Europe. Relative to the climatological mean, the reduction in cyclogenesis over the Gulf Stream is approximately 10% and the increase leeward of the Rocky Mountains is approximately 32% (Table 1). The corresponding signal in cyclone frequency downstream is, however, weak, suggesting that these cyclones have a relatively short lifetime and do not propagate downstream.

During CP El Niño winters (Fig. 7b), anomalies in cyclogenesis frequency are reversed in the three key cyclogenesis regions compared to La Niña winters. We find reduced cyclogenesis frequencies leeward of the Rocky Mountains and at Greenland, whereas the cyclogenesis frequencies are enhanced over the Gulf Stream region (Fig. 7b). However, there are also enhanced cyclogenesis frequencies in the Nordic seas, as for La Niña. Anomalies in cyclone frequency (black

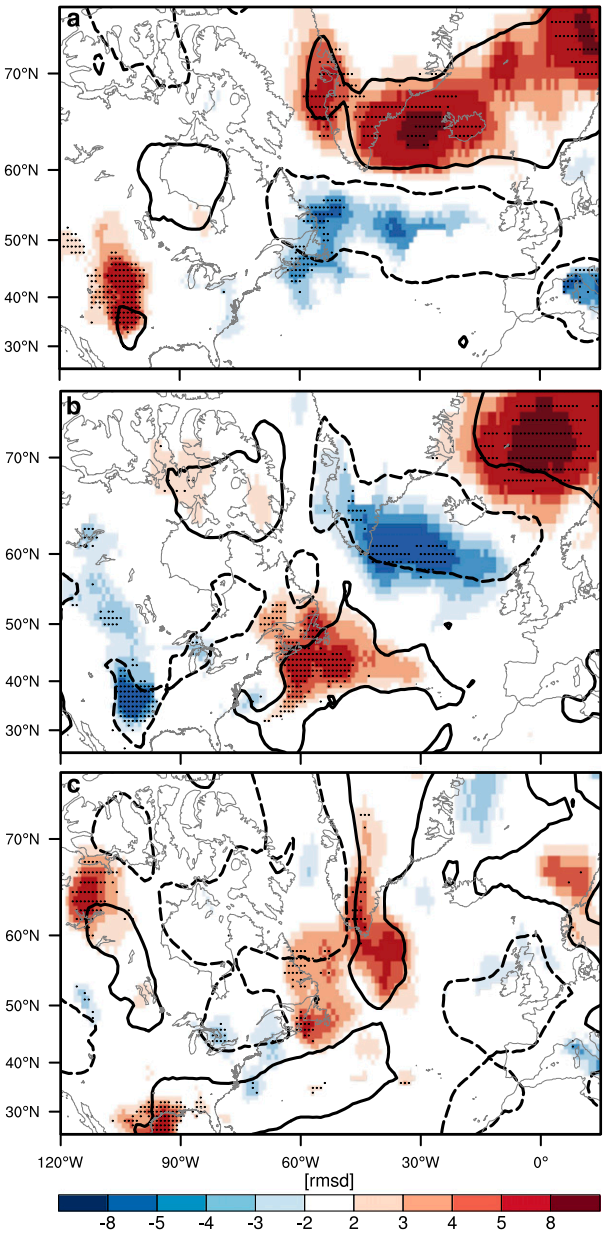

FIG. 7. Standardized cyclogenesis (color; units: root-mean-square deviation from climatological mean) and cyclone frequency anomalies (black contours; units: root-mean-square deviation from climatological mean, −1 (dashed) and +1 (solid) RMSD for (a) La Niña, (b) CP El Niño, and (c) EP El Niño winters. Stippling indicates field-significant grid points (tested through control of the false discovery rate). Shown are only grid points where the climatological cyclogenesis frequency is detected at least at 0.5% of all time steps.

contours) are consistent with anomalies in cyclogenesis frequencies (shading), although the effects seem not to extend as far downstream. There is also a modest signal over North America, with fewer cyclones in the band extending from the central United States across the Great Lakes to Québec, Canada. Relative to the climatological mean, the increase in cyclogenesis over the Gulf Stream is approximately 11% and the decrease leeward of the Rocky Mountains is approximately 27% (Table 1).

TABLE 1. Change in Rocky Mountain, Gulf Stream, and Greenland cyclogenesis relative to the climatological mean for various ENSO phases.

	Rocky Mountain	Gulf Stream	Greenland
La Niña	+32%	−10%	+6%
CP Niño	−27%	+11%	−7%
EP Niño	±0%	±0%	+8%

The situation during EP El Niño winters is less clear. There is slightly enhanced cyclogenesis in the Gulf Stream region (Fig. 7c), similar to CP El Niño winters (Fig. 7b). But otherwise, the EP El Niño cyclogenesis anomalies are much patchier, with enhancements over northern Canada and the Gulf of Mexico. Only for the cyclogenesis anomaly over the Gulf of Mexico, is there a clear downstream signal in total cyclone frequencies. The associated Gulf of Mexico cyclogenesis anomaly is near the North Atlantic jet entrance (e.g., located near the westerly anomaly in the background flow wind; see the black solid contour in Fig. 5a), but located upstream of the climatologically preferred region for Gulf Stream jet entrance cyclogenesis (cf. Fig. 1).

1) FIELD SIGNIFICANCE TEST

To assess the significance of the ENSO-related cyclogenesis anomalies, we compare them against a randomized distribution of cyclogenesis anomalies. The distribution is obtained from a large ensemble of composites, each of which contains the same number of events as the corresponding ENSO composite, populated by randomly selected seasons instead of ENSO seasons. If, for example, a positive cyclogenesis anomaly in the La Niña composite is above the 95th percentile of the randomized distribution, the chance that this anomaly is a random result is below 5%. This corresponds to a p value of 0.1 for a two-sided test since the sign of the anomaly is not known a priori. Every grid point in the map of ENSO-related cyclogenesis anomalies receives a p value relative to the randomized distribution. We then control for the false discovery rate in our entire domain following Wilks (2016). For a control level of $\alpha = 0.1$ (see methods section), we calculate a global p value $p^* = 0.05$ for CP/EP winters and $p^* = 0.04$ for La Niña winters. Cyclogenesis anomalies in Fig. 7 are considered significant if the local p value is less than p^* (this is a stricter measure of significance than using $p < 0.1$).

The field significance test indicates that ENSO-related anomalies are mostly significant during La Niña and CP El Niño winters downstream of the Rocky Mountains, over the Gulf Stream, and at Greenland (Figs. 7a,b), but less so during EP El Niño winters (Fig. 7c).

2) CHANGING THE ODDS IN SURFACE CYCLOGENESIS FREQUENCY

The field significance results give some indication that there are changes in extratropical cyclogenesis over North America and the North Atlantic during different phases of ENSO. To test if there is a systematic change in the probability of seasons with higher/lower than normal cyclogenesis, we compute bootstrapped ensembles (random sampling with replacement) from all winter seasons with high ($\geq$0.5), low (≤ -0.5), and neutral ONI values (see method section for more details). Figure 8a suggests that we can expect enhanced Rocky Mountains cyclogenesis during winters with low ONI (La Niña) relative to winters with high ONI (El Niño), with a shift in mean cyclogenesis events of almost one standard deviation (computed from all winters). For the Gulf Stream (Fig. 8b), we can expect enhanced cyclogenesis during winters with high ONI (El Niño) relative to those with low ONI (La Niña), again with a mean shift of about one standard deviation. The influence on Greenland cyclogenesis is weakest (Fig. 8c), with a modest increase seen for low ONI winters. High-ONI winters exhibit a similar distribution to neutral winters, likely because EP and CP El Niño have opposite effects on Greenland cyclogenesis (Figs. 7b,c).

b. Background flow anomalies for ENSO phases

The various ENSO phases have been shown to be associated with changes in cyclogenesis in the lee of the Rocky Mountains, over the Gulf Stream, and at the southern tip of Greenland (cf. Fig. 7 and Table 1). Now, we examine the link to large-scale flow anomalies seen in seasonal-mean composites of the various ENSO phases.

During La Niña winters, the background wind anomalies are consistent with those that precede Rocky Mountain and Gulf Stream cyclogenesis. As during Rocky Mountain cyclogenesis (Fig. 9b), La Niña winters (Fig. 9a) exhibit a zonal band of enhanced westerlies that extends from the Bay of Alaska toward the west coast of North America, indicating a more active subpolar jet across the Pacific consistent with earlier results (Trenberth et al. 1998; NOAA 2005). Over the North Atlantic, background flow anomalies in the La Niña seasonal-mean composite (Fig. 9a) resemble those during Greenland cyclogenesis (Fig. 9c), with a band of enhanced westerlies extending across the North Atlantic (Fig. 9c), consistent with a poleward-shifted jet.

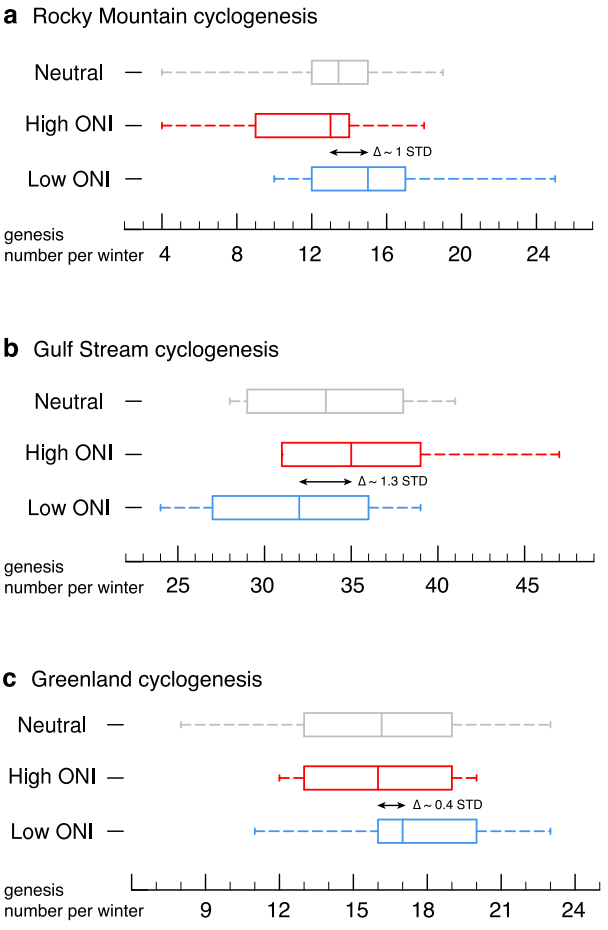

FIG. 8. Bootstrapped distribution of cyclogenesis numbers for (a) Rocky Mountain, (b) Gulf Stream, and (c) Greenland during winters with high ocean Niño index (red; ONI $\geq$ 0.5, corresponding to El Niño), low ONI (blue; ≤ -0.5, corresponding to La Niña), and neutral ONI (gray) cases. Whiskers range between the minimum and the maximum values. Box spans the interquantile range. Vertical line inside each box indicates the median value. The shift between high and low ONI medians is indicated by a black arrow and measured by the standard deviation from the climatological mean. See method section for bootstrapping details.

For El Niño, both CP and EP events exhibit background flow anomalies reminiscent of a zonally extended Pacific jet stream (Figs. 10b,d), which is known to be characteristic for El Niño winters (Trenberth et al. 1998; NOAA 2005). However, the comparison to the background wind anomalies that precede Gulf Stream cyclogenesis (Figs. 10a,c), which is favored during El Niño, is not as compelling as in the case of La Niña. Still, there is a consistent dipole pattern with enhanced westerlies on the equatorward flank of the jet and weakened westerlies on the poleward flank. In addition, there is a consistent northeastward displacement of background flow anomalies from EP El Niño to CP El Niño from the jet entrance to the jet exit region (Figs. 10b,d).

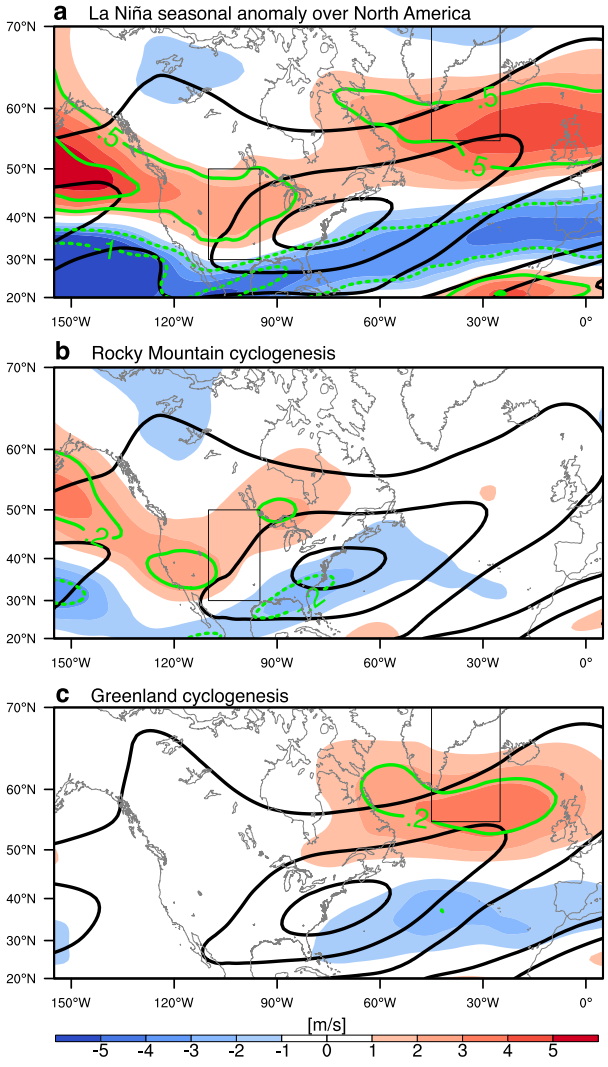

FIG. 9. Composite of (a) La Niña seasonal-mean background wind and anomaly (black contours; 15, 25, and 35 m s^{-1}, 10-day low-pass zonal wind) and its deviation from its climatological mean (color). Composite for (b) Rocky Mountain cyclogenesis background wind and anomaly (at zero lag) with similar contours as in (a). (c) As in (b), but for Greenland cyclogenesis. All fields are vertically averaged between 400 and 200 hPa. Green contours indicates background wind anomalies but standardized (see text for details).

Once again, comparing to large ensembles (10^5) of randomized background flow composites, we find that the background flow anomalies in the cyclogenesis composites (Figs. 9a,c and 10a,c) are on the order of ±3 standard deviations (of the corresponding randomized ensemble) in all three examined regions (see green contours). The seasonal-mean background flow anomalies during ENSO-affected winters (Figs. 9a and 10b,d) are on the order of 0.5–1 standard deviations of the seasonal means of the 37 winters available in the ERA-Interim period.

Regarding decadal variability, we would like to note that there is an increase in the number of CP El Niño events during the second half of the record, raising the possibility that decadal variations play a role in creating the differences observed in the composites of the two types of El Niño events in Fig. 10. Repeating the composite analysis with lower-frequency variations filtered out (8-yr high-pass filter) yields very similar results (not shown), suggesting that the influence of decadal variability is small. This is consistent with the study of Varino et al. (2018), which indicates that Northern Hemisphere extratropical cyclones are only weakly affected by decadal variability during the period 1980–2010 (our study period is 1979–2014).

5. On the formation of cyclogenesis-conducive background flow anomalies during ENSO

Finally, this section probes the mechanisms by which the background flow is modified during ENSO-affected winters to promote changes in cyclogenesis over the various regions that feed the North Atlantic storm track (section 4b and Table 1). In particular, we explore the relative roles of stationary and transient wave propagation in setting the large-scale background flow anomalies that seem to be conducive for cyclogenesis during La Niña and CP El Niño winters, the two seasons for which the cyclogenesis anomalies are clearest and of opposite sign. As this is a purely diagnostic study, we cannot quantitatively attribute the observed cyclogenesis differences to changes in and interactions between stationary and transient waves. However, in using diagnostics that closely track the dynamics of wave–mean flow interactions, we believe the results can offer useful new insights into the important mechanisms at play.

a. La Niña

During La Niña winters (Fig. 11a), anomalous stationary wave propagation is mainly of tropical origin and indicates that stationary waves help to maintain the streamfunction anomalies over the Pacific, as demonstrated in previous studies (Nakamura 1994; Nakamura et al. 1997; Takaya and Nakamura 2001). The stationary wave activity flux points northward around the date line, turns northeastward in midlatitudes, and dissipates over western Canada. The associated streamfunction anomaly over the Pacific–North America sector (Fig. 11a; red shading) shows an intensification of the climatological ridge over the west coast of North America. A northwest–southeast band of enhanced zonal wind stretches across the Pacific–North America sector. This zonal wind anomaly is in close agreement with the background flow

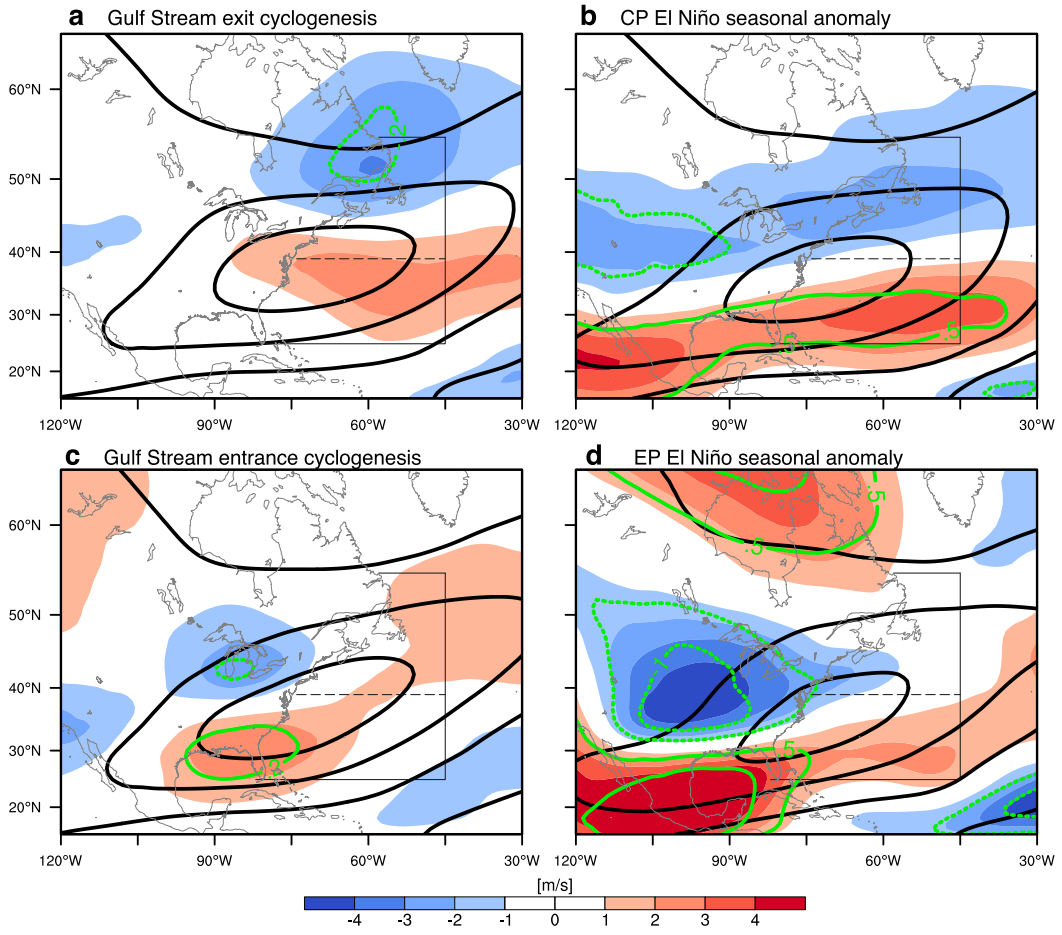

FIG. 10. Composite of (a) Gulf Stream entrance cyclogenesis background wind (black contours; 15, 25, 35, and 45 m s^{-1}, 10-day low-pass zonal wind) and its deviation from the climatological mean (color). (b) EP El Niño seasonal background wind and anomaly with similar contours as in (a). (c) As in (a), but for Gulf Stream exit cyclogenesis. (d) As in (b), but for CP El Niño seasons. All fields are vertically averaged between 400 and 200 hPa. Green contours indicate background wind anomalies but they are standardized.

anomaly seen in the Rocky Mountain cyclogenesis composite (cf. Fig. 9a).

The **E** vectors suggest an additional contribution by transient eddies to the formation of the zonal wind anomalies over the eastern North Pacific (Figs. 12a,b). Here, enhanced **E** vector divergence associated with the more equatorward-oriented **E** vectors (red shading in Fig. 12b) indicates eddy momentum flux convergence caused by transient eddy activity, and collocates with an enhancement of the zonal wind in the eastern North Pacific.

While there is no indication for an anomalous downstream propagation of stationary Rossby waves into the North Atlantic that would potentially contribute to the formation of background flow anomalies at Greenland (Fig. 11a), the **E** vectors suggest an important contribution by transient upper-level eddies (Fig. 12a). The **E** vectors point stronger equatorward, relative to the climatology, indicating a stronger anticyclonic orientation of downstream propagating transient eddies from North America into the North Atlantic (yellow shading in Fig. 12a). Over the North Atlantic, enhanced **E** vector divergence relative to the climatology (red shading in Fig. 12b) indicates an increase in eddy momentum flux convergence, suggesting a contribution by transient eddies to the formation of the background flow anomaly at Greenland (solid black contours in Fig. 12b). The simultaneous eddy momentum flux divergence that extends along a zonal band at 30°N (blue shading in Fig. 12b) shows the transient eddies' contribution to weakening of the background flow (dashed black contours in Fig. 12b). Over the North Atlantic, this pattern resembles a poleward-shifted eddy-driven jet.

b. CP El Niño

During CP El Niño winters, anomalous stationary wave propagation is of tropical origin with an additional

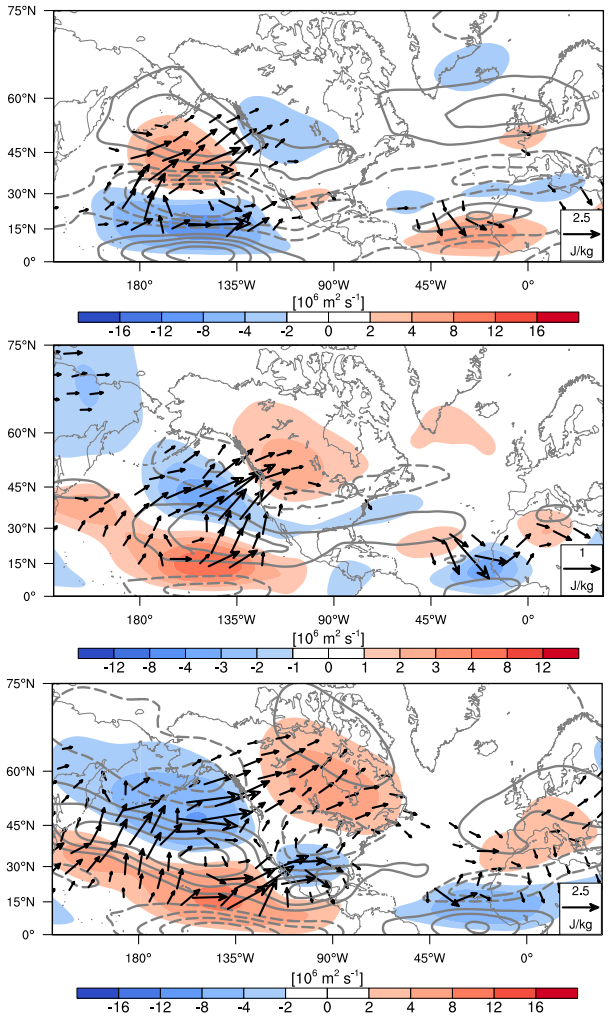

FIG. 11. The 300-hPa stationary wave activity flux (arrows; J kg^{-1}) for (a) La Niña, (b) CP El Niño, and (c) EP El Niño winters. Additionally shown are the corresponding stationary streamfunction (color; 10^6 m^2 s^{-1}) and background flow anomalies (gray contours; solid positive and dashed negative values from -8 to 8 m s^{-1} by 2 m s^{-1}, zero contour omitted).

contribution from subtropical sources upstream of the international date line (Fig. 11b). The stationary wave train from the tropics propagates northward and dissipates over a ridge anomaly (positive streamfunction) over Canada. The wave activity fluxes converge into the negative streamfunction anomaly (i.e., a trough anomaly) near the the Bay of Alaska, which acts to weaken the climatological ridge over the east Pacific and results in more zonal westerlies and a marked extension of the Pacific jet at 30°N. Similar to La Niña, there is no clear signal of a downstream propagation of stationary waves into the North Atlantic.

The anomalous **E** vector convergence (corresponding to momentum flux divergence) over the Bay of Alaska (blue shading in Fig. 12d) suggests a contribution from transient upper-level eddies to the weakening of the background flow and the climatological ridge in this sector. The **E** vectors over the eastern North Pacific and over North America are less equatorward pointing relative to the climatological mean (blue shading in Fig. 12c). Downstream over the Gulf Stream the **E** vectors point more poleward across the entire North Atlantic relative to the climatological mean and La Niña (blue shading in Fig. 12c). The associated eddy momentum flux convergence is anomalously equatorward as suggested by the anomalous **E** vector divergence pattern (Fig. 12d); acting to shift the North Atlantic jet equatorward over the western North Atlantic.

To conclude on CP El Niño, both the anomalous quasi-stationary wave and transient waves play a key role in the formation of background flow anomalies in the eastern North Pacific that are less favorable to Rocky Mountain cyclogenesis. The anomalous quasi-stationary wave train has less amplitude over the U.S. East Coast, which suggests that its contribution to Gulf Stream cyclogenesis-conducive background flow anomalies is less important than transient eddies. Farther downstream, near 45°N, the background flow anomalies that are less favorable to Greenland cyclogenesis are more likely due to transient waves only.

c. *EP El Niño*

The situation for EP El Niño winters is less clear. The reflection of the easternmost stationary wave train back into the tropics over the Gulf of Mexico complicates the situation (Fig. 11c), but the large-scale trough anomaly over the northeast Pacific is similar to that during CP Niño winters. However, over the Gulf Stream and in the North Atlantic, no coherent picture emerges from the **E** vectors (Figs. 12e,f).

Our findings are consistent with earlier studies that have highlighted the relative importance of propagating transient eddies in setting the North Atlantic circulation response during ENSO. As suggested in Drouard et al. (2013) and Drouard et al. (2015), a Pacific ridge anomaly during La Niña reinforces the equatorward orientation of transient upper-level eddies over North America relative to the climatological mean. In other words, upper-level eddies have more of an anticyclonic (southwest–northeast) tilt during La Niña winters, which was found to result in more anticyclonic wave breaking in the North Atlantic and a poleward-shifted North Atlantic jet. In addition our separation of CP and EP El Niño events highlights that a North Atlantic teleconnection opposite to that seen during La Niña winters emerges in particular for CP El Niño winters. Further, our study supports the idea that stationary Rossby waves do not play a direct role in setting the North Atlantic teleconnection, but may

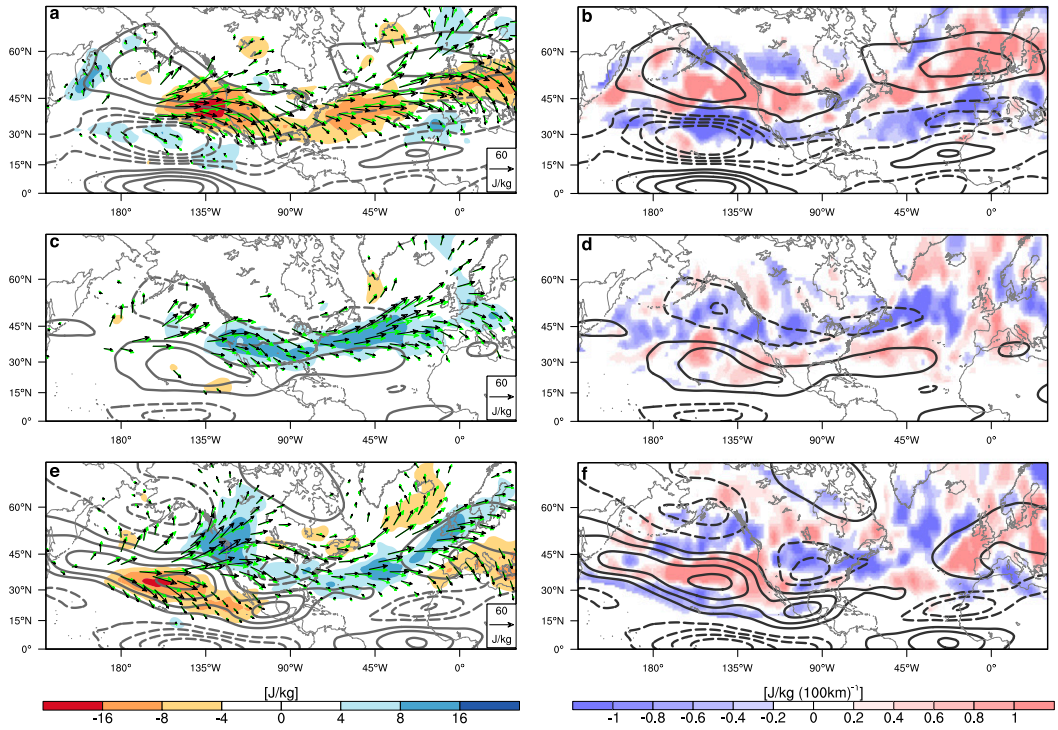

FIG. 12. (left) The 300-hPa **E** vectors (black arrows; J kg^{-1}) for (a) La Niña, (c) CP El Niño, and (e) EP El Niño winters, **E** vector climatological mean (green arrows), difference in their meridional component (color; blue indicates stronger poleward orientation and red stronger equatorward orientation), and background flow anomaly (gray contours; solid positive and dashed negative values from −8 to 8 m s^{-1} by 2 m s^{-1}, zero contour omitted). (right) Anomalous **E** vector divergence [shading; J kg^{-1} (100 km)$^{-1}$] and background flow anomalies (as in left column) for (b) La Niña, (d) CP El Niño, and (f) EP El Niño winters.

indirectly contribute to it by altering the propagation characteristics of transient eddies and how they will deposit momentum in the North Atlantic.

6. Summary

This study investigates the dynamics of transient eddies and stationary waves in setting the tropospheric ENSO teleconnections to the North Atlantic during boreal winter (DJF) and their relative roles in the formation of cyclogenesis-conducive background flow anomalies. The results further explored the linkages between ENSO-related background wind anomalies and extratropical surface cyclogenesis in three regions feeding into the North Atlantic surface storm track: the lee of the Rocky Mountains, over the Gulf Stream, and south of Greenland.

We observe the following relationships between extratropical cyclogenesis and ENSO (Table 1). During La Niña winters, Rocky Mountain cyclogenesis is enhanced by over 30% and Greenland cyclogenesis is enhanced by 6%; Gulf Stream cyclogenesis is reduced by 10%. During CP El Niño winters, the situation is reversed, with anomalies of approximately the same amplitude. Bootstrapping suggests that the observed cyclogenesis anomalies for La Niña and CP El Niño are robust, while EP El Niño winters show weak anomalies with large uncertainties (Fig. 7).

The presented results augment previous findings about the tropospheric ENSO pathway and what emerges is a richer picture of the dynamics at play during ENSO-affected winters. The schematic in Fig. 13 summarizes the investigated mechanisms for the observed cyclogenesis anomalies, which form a plausible and consistent picture but cannot be viewed as conclusive in the absence of further modeling experiments.

- During La Niña winters (Fig. 13a), our analysis suggests that stationary and transient wave propagation contribute to the formation of seasonal-mean flow anomalies like those occurring prior to Rocky Mountain cyclogenesis, with a stronger subpolar jet (left red arrow) and an enhanced ridge over the northeastern Pacific. The enhanced ridge is associated with transient upper-level eddies that propagate with a stronger equatorward orientation across North America and the North Atlantic (resulting in more anticyclonic wave breaking, see also Drouard et al. 2015), as indicated by the equatorward-oriented **E** vectors

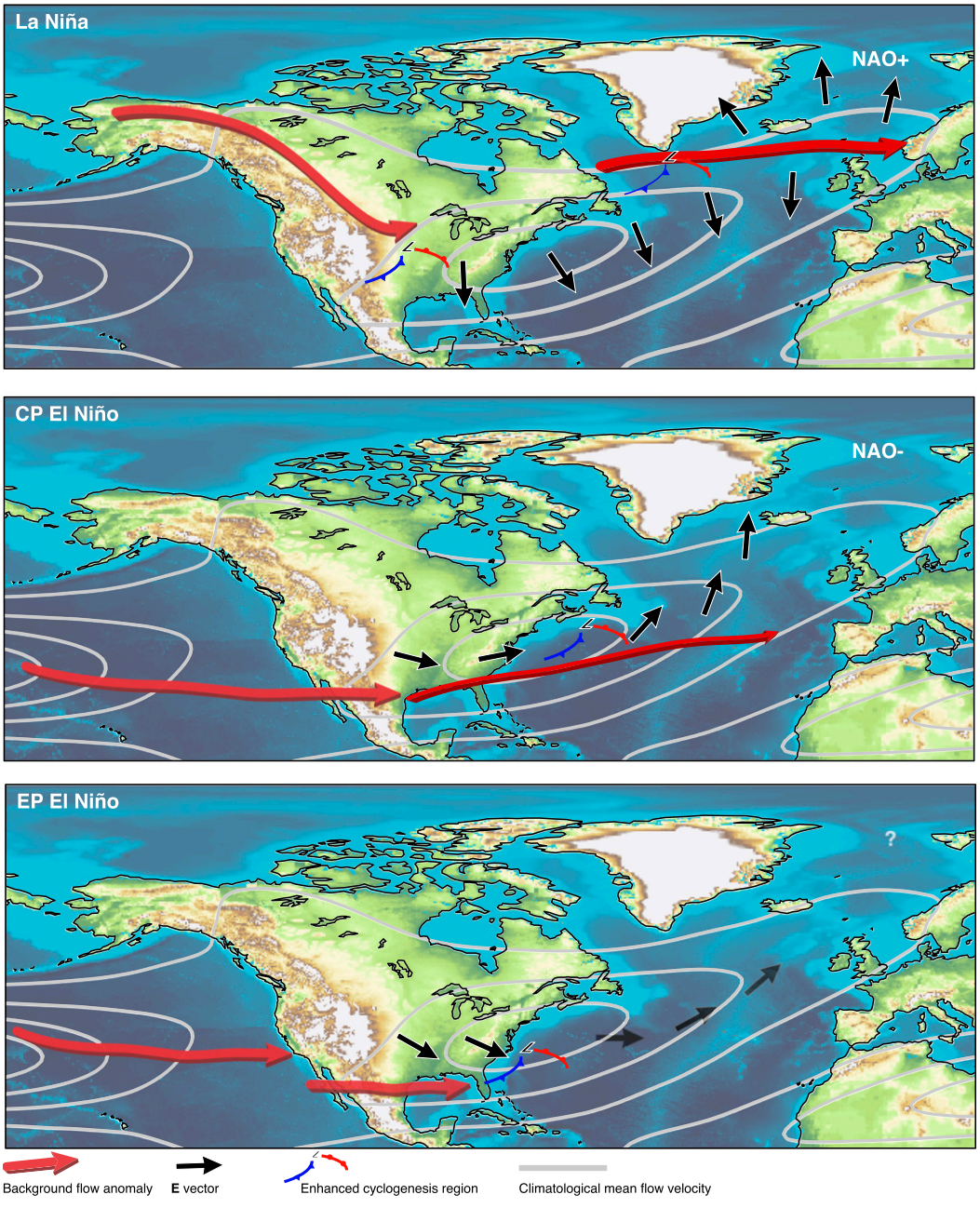

FIG. 13. Schematic representation of the dynamical building blocks underlying a plausible and consistent potential *tropospheric* ENSO pathway during (a) La Niña and (b) CP and (c) EP El Niño winters. Shown are background flow anomalies at the jet-stream level (red arrows), the 300-hPa winter mean flow (gray contours), **E** vectors, and the identified preferred locations of extratropical cyclogenesis (cyclone symbols). The North Atlantic circulation response to La Niña and CP El Niño tends to be of opposite sign. For EP El Niño winters, the situation is more uncertain.

(black arrows). The associated anomalous eddy momentum flux convergences would act to push the eddy-driven jet stream poleward (right red arrow), consistent with large-scale flow anomalies that precede Greenland cyclogenesis. This poleward migration of the North Atlantic jet is also consistent with a positive late-winter NAO-like response during La Niña winters identified in previous studies (Li and Lau 2012b,a; Drouard et al. 2015), though it is unclear whether an actual NAO event is triggered (García-Serrano et al. 2011). The observed cyclogenesis changes at Greenland, however, are modest, suggesting an important role for additional mechanisms controlling Greenland cyclogenesis (e.g., low-level cold-air advection).

- During CP El Niño winters (Fig. 13b), our analysis suggests that stationary and transient wave propagation contribute to the formation of seasonal-mean flow anomalies like those occurring prior to Gulf Stream cyclogenesis. The stationary and transient waves induce a zonally extended Pacific jet (left red arrow) and a weak ridge over the northeastern Pacific. The role of the stationary wave weakens downstream over North America and is negligible over the North Atlantic. The equatorward-shifted jet in the western North Atlantic, which is a favorable situation for Gulf Stream exit cyclogenesis, is shown to be partly due the stationary and transient waves. The stronger poleward propagation of transient upper-level eddies (black arrows) from North America downstream over the North Atlantic and associated anomalous eddy momentum flux divergence help to push the North Atlantic jet equatorward, consistent with a negative late-winter NAO-like response (Li and Lau 2012b,a; Drouard et al. 2015).
- During EP El Niño winters (Fig. 13c), the large-scale circulation response in the North Pacific is similar to that during CP El Niño winters, but cyclogenesis and North Atlantic circulation signals are weak.

The analyses presented here aim for a better understanding of the coupling between tropical Pacific SST variability and the North Atlantic storm track through changes in cyclogenesis. The results are clearest for La Niña and CP El Niño events, suggesting that ENSO diversity (Capotondi et al. 2015) and the relative low number of events could be a factor in the ongoing struggle to isolate the ENSO-related extratropical circulation response outside the Pacific sector (Deser et al. 2017). The number of cyclones within the North Atlantic storm track is inherently linked to the number of cyclogenesis events, but a range of other synoptic to large-scale influences should be considered, including variability in cyclolysis and the interaction between the troposphere and stratosphere. Future work may also address differences in the cyclogenesis response to tropical forcing during late fall versus early winter (King et al. 2018), or whether the mechanisms described here are subject to multidecadal variability (Varino et al. 2018).

Acknowledgments. Sebastian Schemm acknowledges funding from the Swiss National Science Foundation (P300P2_167745 and P323P2_167747). Gwendal Rivière acknowledges funding from the ANR (Project GOTHAM; ANR-15-JCLI-0004). The study was supported by the Norwegian Research Council Project DynAMiTe 255027. We acknowledge the helpful comments of two anonymous reviewers and the editor, Walter Robinson.

REFERENCES

Alexander, M. A., I. Bladé, M. Newman, J. R. Lanzante, N. Lau, and J. D. Scott, 2002: The atmospheric bridge: The influence of ENSO teleconnections on air–sea interaction over the global oceans. *J. Climate*, **15**, 2205–2231, https://doi.org/10.1175/1520-0442(2002)015<2205:TABTIO>2.0.CO;2.

Ashok, K., S. K. Behera, S. A. Rao, H. Weng, and T. Yamagata, 2007: El Niño Modoki and its possible teleconnection. *J. Geophys. Res.*, **112**, C11007, https://doi.org/10.1029/2006JC003798.

Bluestein, H. B., 1993: *Synoptic-Dynamic Meteorology in Midlatitudes*. Vol. II, *Observations and Theory of Weather Systems,* Oxford University Press, 594 pp.

Branstator, G., 1985: Analysis of general circulation model sea-surface temperature anomaly simulations using a linear model. Part I: Forced solutions. *J. Atmos. Sci.*, **42**, 2225–2241, https://doi.org/10.1175/1520-0469(1985)042<2225:AOGCMS>2.0.CO;2.

——, 2014: Long-lived response of the midlatitude circulation and storm tracks to pulses of tropical heating. *J. Climate*, **27**, 8809–8826, https://doi.org/10.1175/JCLI-D-14-00312.1.

Brönnimann, S., J. Luterbacher, J. Staehelin, T. M. Svendby, G. Hansen, and T. Svenøe, 2004: Extreme climate of the global troposphere and stratosphere in 1940–42 related to El Niño. *Nature*, **431**, 971–974, https://doi.org/10.1038/nature02982.

——, E. Xoplaki, C. Casty, A. Pauling, and J. Luterbacher, 2007: ENSO influence on Europe during the last centuries. *Climate Dyn.*, **28**, 181–197, https://doi.org/10.1007/s00382-006-0175-z.

Butler, A. H., L. M. Polvani, and C. Deser, 2014: Separating the stratospheric and tropospheric pathways of El Niño–Southern Oscillation teleconnections. *Environ. Res. Lett.*, **9**, 024014, https://doi.org/10.1088/1748-9326/9/2/024014.

Capotondi, A., and Coauthors, 2015: Understanding ENSO diversity. *Bull. Amer. Meteor. Soc.*, **96**, 921–938, https://doi.org/10.1175/BAMS-D-13-00117.1.

Chang, E. K. M., 1993: Downstream development of baroclinic waves as inferred from regression analysis. *J. Atmos. Sci.*, **50**, 2038–2053, https://doi.org/10.1175/1520-0469(1993)050<2038:DDOBWA>2.0.CO;2.

Ciasto, L. M., and D. W. J. Thompson, 2008: Observations of large-scale ocean–atmosphere interaction in the Southern Hemisphere. *J. Climate*, **21**, 1244–1259, https://doi.org/10.1175/2007JCLI1809.1.

——, C. Li, J. J. Wettstein, and N. G. Kvamstø, 2016: North Atlantic storm-track sensitivity to projected sea surface temperature: Local versus remote influences. *J. Climate*, **29**, 6973–6991, https://doi.org/10.1175/JCLI-D-15-0860.1.

Clark, A. J., C. J. Schaffer, W. A. Gallus Jr., and K. Johnson-O'Mara, 2009: Climatology of storm reports relative to upper-level jet streaks. *Wea. Forecasting*, **24**, 1032–1051, https://doi.org/10.1175/2009WAF2222216.1.

Deser, C., I. R. Simpson, K. A. McKinnon, and A. S. Phillips, 2017: The Northern Hemisphere extratropical atmospheric circulation response to ENSO: How well do we know it and how do we evaluate models accordingly? *J. Climate*, **30**, 5059–5082, https://doi.org/10.1175/JCLI-D-16-0844.1.

Ding, Q., J. M. Wallace, D. S. Battisti, E. J. Steig, A. J. E. Gallant, H.-J. Kim, and L. Geng, 2014: Tropical forcing of the recent rapid Arctic warming in northeastern Canada and Greenland. *Nature*, **509**, 209–212, https://doi.org/10.1038/nature13260.

——, and Coauthors, 2017: Influence of high-latitude atmospheric circulation changes on summertime Arctic sea ice. *Nat. Climate Change*, **7**, 289–295, https://doi.org/10.1038/nclimate3241.

Domeisen, D. I. V., A. H. Butler, K. Fröhlich, M. Bittner, W. A. Müller, and J. Baehr, 2015: Seasonal predictability over Europe arising from El Niño and stratospheric variability in the MPI-ESM seasonal prediction system. *J. Climate*, **28**, 256–271, https://doi.org/10.1175/JCLI-D-14-00207.1.

Drouard, M., G. Rivière, and P. Arbogast, 2013: The North Atlantic Oscillation response to large-scale atmospheric anomalies in the northeastern Pacific. *J. Atmos. Sci.*, **70**, 2854–2874, https://doi.org/10.1175/JAS-D-12-0351.1.

——, ——, and ——, 2015: The link between the North Pacific climate variability and the North Atlantic Oscillation via downstream propagation of synoptic waves. *J. Climate*, **28**, 3957–3976, https://doi.org/10.1175/JCLI-D-14-00552.1.

Eichler, T., and W. Higgins, 2006: Climatology and ENSO-related variability of North American extratropical cyclone activity. *J. Climate*, **19**, 2076–2093, https://doi.org/10.1175/JCLI3725.1.

Exner, F., 1914: Über monatliche Witterungsanomalien auf der nördlichen Halbkugel im Winter (On monthly weather anomalies in the Northern Hemisphere in winter). *Meteor. Z.*, **31**, 104–109, https://doi.org/10.1127/metz/2015/0654.

Frauen, C., D. Dommenget, N. Tyrrell, M. Rezny, and S. Wales, 2014: Analysis of the nonlinearity of El Niño–Southern Oscillation teleconnections. *J. Climate*, **27**, 6225–6244, https://doi.org/10.1175/JCLI-D-13-00757.1.

García-Serrano, J., B. Rodríguez-Fonseca, I. Bladé, P. Zurita-Gotor, and A. de la Cámara, 2011: Rotational atmospheric circulation during North Atlantic–European winter: The influence of ENSO. *Climate Dyn.*, **37**, 1727–1743, https://doi.org/10.1007/s00382-010-0968-y.

Garfinkel, C. I., and D. L. Hartmann, 2008: Different ENSO teleconnections and their effects on the stratospheric polar vortex. *J. Geophys. Res.*, **113**, D18114, https://doi.org/10.1029/2008JD009920.

——, A. H. Butler, D. W. Waugh, M. M. Hurwitz, and L. M. Polvani, 2012: Why might stratospheric sudden warmings occur with similar frequency in El Niño and La Niña winters? *J. Geophys. Res.*, **117**, D19106, https://doi.org/10.1029/2012JD017777.

——, M. M. Hurwitz, D. W. Waugh, and A. H. Butler, 2013a: Are the teleconnections of central Pacific and eastern Pacific El Niño distinct in boreal wintertime? *Climate Dyn.*, **41**, 1835–1852, https://doi.org/10.1007/s00382-012-1570-2.

——, D. W. Waugh, and E. P. Gerber, 2013b: The effect of tropospheric jet latitude on coupling between the stratospheric polar vortex and the troposphere. *J. Climate*, **26**, 2077–2095, https://doi.org/10.1175/JCLI-D-12-00301.1.

Gershunov, A., and T. P. Barnett, 1998: ENSO influence on intraseasonal extreme rainfall and temperature frequencies in the contiguous United States: Observations and model results. *J. Climate*, **11**, 1575–1586, https://doi.org/10.1175/1520-0442(1998)011<1575:EIOIER>2.0.CO;2.

Graf, H.-F., and D. Zanchettin, 2012: Central Pacific El Niño, the "subtropical bridge," and Eurasian climate. *J. Geophys. Res.*, **117**, D01102, https://doi.org/10.1029/2011JD016493.

Graf, M. A., H. Wernli, and M. Sprenger, 2017: Objective classification of extratropical cyclogenesis. *Quart. J. Roy. Meteor. Soc.*, **143**, 1047–1061, https://doi.org/10.1002/qj.2989.

Greatbatch, R. J., J. Lu, and K. A. Peterson, 2004: Nonstationary impact of ENSO on Euro-Atlantic winter climate. *Geophys. Res. Lett.*, **31**, L02208, https://doi.org/10.1029/2003GL018542.

Halpert, M. S., and C. F. Ropelewski, 1992: Surface temperature patterns associated with the Southern Oscillation. *J. Climate*, **5**, 577–593, https://doi.org/10.1175/1520-0442(1992)005<0577:STPAWT>2.0.CO;2.

Hardiman, S. C., and P. H. Haynes, 2008: Dynamical sensitivity of the stratospheric circulation and downward influence of upper level perturbations. *J. Geophys. Res.*, **113**, D23103, https://doi.org/10.1029/2008JD010168.

Held, I. M., S. W. Lyons, and S. Nigam, 1989: Transients and the extratropical response to El Niño. *J. Atmos. Sci.*, **46**, 163–174, https://doi.org/10.1175/1520-0469(1989)046<0163:TATERT>2.0.CO;2.

——, M. Ting, and H. Wang, 2002: Northern winter stationary waves: Theory and modeling. *J. Climate*, **15**, 2125–2144, https://doi.org/10.1175/1520-0442(2002)015<2125:NWSWTA>2.0.CO;2.

Hoerling, M. P., and A. Kumar, 2002: Atmospheric response patterns associated with tropical forcing. *J. Climate*, **15**, 2184–2203, https://doi.org/10.1175/1520-0442(2002)015<2184:ARPAWT>2.0.CO;2.

Holton, J. R., 2004: *An Introduction to Dynamic Meteorology*. 4th ed. Academic Press, 535 pp.

Honda, M., H. Nakamura, J. Ukita, I. Kousaka, and K. Takeuchi, 2001: Interannual seesaw between the Aleutian and Icelandic lows. Part I: Seasonal dependence and life cycle. *J. Climate*, **14**, 1029–1042, https://doi.org/10.1175/1520-0442(2001)014<1029:ISBTAA>2.0.CO;2.

Horel, J. D., and J. M. Wallace, 1981: Planetary-scale atmospheric phenomena associated with the Southern Oscillation. *Mon. Wea. Rev.*, **109**, 813–829, https://doi.org/10.1175/1520-0493(1981)109<0813:PSAPAW>2.0.CO;2.

Hoskins, B. J., and D. J. Karoly, 1981: The steady linear response of a spherical atmosphere to thermal and orographic forcing. *J. Atmos. Sci.*, **38**, 1179–1196, https://doi.org/10.1175/1520-0469(1981)038<1179:TSLROA>2.0.CO;2.

——, and T. Ambrizzi, 1993: Rossby wave propagation on a realistic longitudinally varying flow. *J. Atmos. Sci.*, **50**, 1661–1671, https://doi.org/10.1175/1520-0469(1993)050<1661:RWPOAR>2.0.CO;2.

——, and K. I. Hodges, 2002: New perspectives on the Northern Hemisphere winter storm tracks. *J. Atmos. Sci.*, **59**, 1041–1061, https://doi.org/10.1175/1520-0469(2002)059<1041:NPOTNH>2.0.CO;2.

——, I. N. James, and G. H. White, 1983: The shape, propagation and mean-flow interaction of large-scale weather systems. *J. Atmos. Sci.*, **40**, 1595–1612, https://doi.org/10.1175/1520-0469(1983)040<1595:TSPAMF>2.0.CO;2.

Hurrell, J. W., 1996: Influence of variations in extratropical wintertime teleconnections on northern hemisphere temperature. *Geophys. Res. Lett.*, **23**, 665–668, https://doi.org/10.1029/96GL00459.

Ineson, S., and A. Scaife, 2009: The role of the stratosphere in the European climate response to El Niño. *Nat. Geosci.*, **2**, 32–36, https://doi.org/10.1038/ngeo381.

Jiménez-Esteve, B., and D. I. Domeisen, 2018: The tropospheric pathway of the ENSO–North Atlantic teleconnection. *J. Climate*, **31**, 4563–4584, https://doi.org/10.1175/JCLI-D-17-0716.1.

Kao, H.-Y., and J.-Y. Yu, 2009: Contrasting eastern-Pacific and central-Pacific types of ENSO. *J. Climate*, **22**, 615–632, https://doi.org/10.1175/2008JCLI2309.1.

Karoly, D. J., R. A. Plumb, and M. Ting, 1989: Examples of the horizontal propagation of quasi-stationary waves. *J. Atmos. Sci.*, **46**, 2802–2811, https://doi.org/10.1175/1520-0469(1989)046<2802:EOTHPO>2.0.CO;2.

King, M. P., I. Herceg-Bulić, I. Bladé, J. García-Serrano, N. Keenlyside, F. Kucharski, C. Li, and S. Sobolowski, 2018: Importance of late fall ENSO teleconnection in the Euro-Atlantic sector. *Bull. Amer. Meteor. Soc.*, **99**, 1337–1343, https://doi.org/10.1175/BAMS-D-17-0020.1.

Li, Y., and N.-C. Lau, 2012a: Contributions of downstream eddy development to the teleconnection between ENSO and the atmospheric circulation over the North Atlantic. *J. Climate*, **25**, 4993–5010, https://doi.org/10.1175/JCLI-D-11-00377.1.

——, and ——, 2012b: Impact of ENSO on the atmospheric variability over the North Atlantic in late winter—Role of transient eddies. *J. Climate*, **25**, 320–342, https://doi.org/10.1175/JCLI-D-11-00037.1.

López-Parages, J., B. Rodríguez-Fonseca, D. Dommenget, and C. Frauen, 2016: ENSO influence on the North Atlantic European climate: A non-linear and non-stationary approach. *Climate Dyn.*, **47**, 2071–2084, https://doi.org/10.1007/s00382-015-2951-0.

Manzini, E., M. A. Giorgetta, M. Esch, L. Kornblueh, and E. Roeckner, 2006: The influence of sea surface temperatures on the northern winter stratosphere: Ensemble simulations with the MAECHAM5 model. *J. Climate*, **19**, 3863–3881, https://doi.org/10.1175/JCLI3826.1.

May, W., and L. Bengtsson, 1998: The signature of ENSO in the Northern Hemisphere midlatitude seasonal mean flow and high-frequency intraseasonal variability. *Meteor. Atmos. Phys.*, **69**, 81–100, https://doi.org/10.1007/BF01025185.

Moron, V., and I. Gouirand, 2003: Seasonal modulation of the El Niño–Southern Oscillation relationship with sea level pressure anomalies over the North Atlantic in October–March 1873–1996. *Int. J. Climatol.*, **23**, 143–155, https://doi.org/10.1002/joc.868.

——, and G. Plaut, 2003: The impact of El Niño–Southern Oscillation upon weather regimes over Europe and the North Atlantic during boreal winter. *Int. J. Climatol.*, **23**, 363–379, https://doi.org/10.1002/joc.890.

Nakamura, H., 1994: Rotational evolution of potential vorticity associated with a strong blocking flow configuration over Europe. *Geophys. Res. Lett.*, **21**, 2003–2006, https://doi.org/10.1029/94GL01614.

——, M. Nakamura, and J. L. Anderson, 1997: The role of high- and low-frequency dynamics in blocking formation. *Mon. Wea. Rev.*, **125**, 2074–2093, https://doi.org/10.1175/1520-0493(1997)125<2074:TROHAL>2.0.CO;2.

NOAA, 2005: El Niño and La Niña-related winter features over North America. NOAA/NWS Climate Prediction Center, accessed 17 August 2017, http://www.cpc.ncep.noaa.gov/products/analysis_monitoring/ensocycle/nawinter.shtml.

Park, H.-S., S. Lee, S.-W. Son, S. B. Feldstein, and Y. Kosaka, 2015: The impact of poleward moisture and sensible heat flux on Arctic winter sea ice variability. *J. Climate*, **28**, 5030–5040, https://doi.org/10.1175/JCLI-D-15-0074.1.

Parker, D. J., 1998: Secondary frontal waves in the North Atlantic region: A dynamical perspective of current ideas. *Quart. J. Roy. Meteor. Soc.*, **124**, 829–856, https://doi.org/10.1002/qj.49712454709.

Plumb, R. A., 1985: On the three-dimensional propagation of stationary waves. *J. Atmos. Sci.*, **42**, 217–229, https://doi.org/10.1175/1520-0469(1985)042<0217:OTTDPO>2.0.CO;2.

——, and K. Semeniuk, 2003: Downward migration of extratropical zonal wind anomalies. *J. Geophys. Res.*, **108**, 4223, https://doi.org/10.1029/2002JD002773.

Polvani, L. M., L. Sun, A. H. Butler, J. H. Richter, and C. Deser, 2017: Distinguishing stratospheric sudden warmings from ENSO as key drivers of wintertime climate variability over the North Atlantic and Eurasia. *J. Climate*, **30**, 1959–1969, https://doi.org/10.1175/JCLI-D-16-0277.1.

Pozo-Vázquez, D., S. R. Gámiz-Fortis, J. Tovar-Pescador, M. J. Esteban-Parra, and Y. Castro-Dez, 2005: El Niño–Southern Oscillation events and associated European winter precipitation anomalies. *Int. J. Climatol.*, **25**, 17–31, https://doi.org/10.1002/joc.1097.

Richter, J. H., C. Deser, and L. Sun, 2015: Effects of stratospheric variability on El Niño teleconnections. *Environ. Res. Lett.*, **10**, 124021, https://doi.org/10.1088/1748-9326/10/12/124021.

Rivière, G., B. L. Hua, and P. Klein, 2003: Perturbation growth in terms of barotropic alignment properties. *Quart. J. Roy. Meteor. Soc.*, **129**, 2613–2635, https://doi.org/10.1256/qj.02.106.

Rodríguez-Fonseca, B., and Coauthors, 2016: A review of ENSO influence on the North Atlantic. A non-stationary signal. *Atmosphere*, **7**, **87**, https://doi.org/10.3390/atmos7070087.

Ropelewski, C. F., and M. S. Halpert, 1987: Global and regional scale precipitation patterns associated with the El Niño/Southern Oscillation. *Mon. Wea. Rev.*, **115**, 1606–1626, https://doi.org/10.1175/1520-0493(1987)115<1606:GARSPP>2.0.CO;2.

Schemm, S., and M. Sprenger, 2015: Frontal-wave cyclogenesis in the North Atlantic—A climatological characterisation. *Quart. J. Roy. Meteor. Soc.*, **141**, 2989–3005, https://doi.org/10.1002/qj.2584.

——, L. M. Ciasto, C. Li, and N. G. Kvamstø, 2016: Influence of tropical Pacific sea surface temperature on the genesis of Gulf Stream cyclones. *J. Atmos. Sci.*, **73**, 4203–4214, https://doi.org/10.1175/JAS-D-16-0072.1.

——, M. Sprenger, and H. Wernli, 2018: When during their life cycle are extratropical cyclones attended by fronts? *Bull. Amer. Meteor. Soc.*, **99**, 149–165, https://doi.org/10.1175/BAMS-D-16-0261.1.

Seager, R., N. Naik, M. Ting, M. A. Cane, N. Harnik, and Y. Kushnir, 2010: Adjustment of the atmospheric circulation to tropical Pacific SST anomalies: Variability of transient eddy propagation in the Pacific–North America sector. *Quart. J. Roy. Meteor. Soc.*, **136**, 277–296, https://doi.org/10.1002/qj.588.

Simmons, A. J., and B. J. Hoskins, 1979: The downstream and upstream development of unstable baroclinic waves. *J. Atmos. Sci.*, **36**, 1239–1254, https://doi.org/10.1175/1520-0469(1979)036<1239:TDAUDO>2.0.CO;2.

Smith, C. A., and P. D. Sardeshmukh, 2000: The effect of ENSO on the intraseasonal variance of surface temperatures in winter. *Int. J. Climatol.*, **20**, 1543–1557, https://doi.org/10.1002/1097-0088(20001115)20:13<1543::AID-JOC579>3.0.CO;2-A.

Sprenger, M., and H. Wernli, 2015: The LAGRANTO Lagrangian analysis tool—Version 2.0. *Geosci. Model Dev.*, **8**, 2569–2586, https://doi.org/10.5194/gmd-8-2569-2015.

——, and Coauthors, 2017: Global climatologies of Eulerian and Lagrangian flow features based on ERA-Interim. *Bull. Amer. Meteor. Soc.*, **98**, 1739–1748, https://doi.org/10.1175/BAMS-D-15-00299.1.

Stan, C., D. M. Straus, J. S. Frederiksen, H. Lin, E. D. Maloney, and C. Schumacher, 2017: Review of tropical-extratropical teleconnections on intraseasonal time scales. *Rev. Geophys.*, **55**, 902–937, https://doi.org/10.1002/2016RG000538.

Takaya, K., and H. Nakamura, 2001: A formulation of a phase-independent wave-activity flux for stationary and migratory quasigeostrophic eddies on a zonally varying basic flow. *J. Atmos. Sci.*, **58**, 608–627, https://doi.org/10.1175/1520-0469(2001)058<0608:AFOAPI>2.0.CO;2.

Toniazzo, T., and A. A. Scaife, 2006: The influence of ENSO on winter North Atlantic climate. *Geophys. Res. Lett.*, **33**, L24704, https://doi.org/10.1029/2006GL027881.

Trenberth, K. E., 1986: An assessment of the impact of transient eddies on the zonal flow during a blocking episode using localized Eliassen–Palm flux diagnostics. *J. Atmos. Sci.*, **43**, 2070–2087, https://doi.org/10.1175/1520-0469(1986)043<2070:AAOTIO>2.0.CO;2.

——, and J. M. Caron, 2000: The Southern Oscillation revisited: Sea level pressures, surface temperatures, and precipitation.

J. Climate, **13**, 4358–4365, https://doi.org/10.1175/1520-0442(2000)013<4358:TSORSL>2.0.CO;2.

——, G. W. Branstator, D. Karoly, A. Kumar, N.-C. Lau, and C. Ropelewski, 1998: Progress during TOGA in understanding and modeling global teleconnections associated with tropical sea surface temperatures. *J. Geophys. Res.*, **103**, 14 291–14 324, https://doi.org/10.1029/97JC01444.

van Loon, H., and R. A. Madden, 1981: The southern oscillation. Part I: Global associations with pressure and temperature in northern winter. *Mon. Wea. Rev.*, **109**, 1150–1162, https://doi.org/10.1175/1520-0493(1981)109<1150:TSOPIG>2.0.CO;2.

Varino, F., P. Arbogast, B. Joly, G. Rivière, M.-L. Fandeur, H. Bovy, and J.-B. Granier, 2018: Northern Hemisphere extratropical winter cyclones variability over the 20th century derived from ERA-20C reanalysis. *Climate Dyn.*, https://doi.org/10.1007/s00382-018-4176-5, in press.

Wernli, H., and C. Schwierz, 2006: Surface cyclones in the ERA-40 dataset (1958–2001). Part I: Novel identification method and global climatology. *J. Atmos. Sci.*, **63**, 2486–2507, https://doi.org/10.1175/JAS3766.1.

Wettstein, J. J., and C. Deser, 2014: Internal variability in projections of twenty-first-century arctic sea ice loss: Role of the large-scale atmospheric circulation. *J. Climate*, **27**, 527–550, doi:10.1175/JCLI-D-12-00839.1.

Wilks, D. S., 2016: ''The stippling shows statistically significant grid points'': How research results are routinely overstated and overinterpreted, and what to do about it. *Bull. Amer. Meteor. Soc.*, **97**, 2263–2273, https://doi.org/10.1175/BAMS-D-15-00267.1.

Yeh, S.-W., J.-S. Kug, B. Dewitte, M.-H. Kwon, B. P. Kirtman, and F.-F. Jin, 2009: El Niño in a changing climate. *Nature*, **461**, 511–514, https://doi.org/10.1038/nature08316.

Yu, J.-Y., Y. Zou, S. T. Kim, and T. Lee, 2012: The changing impact of El Niño on US winter temperatures. *Geophys. Res. Lett.*, **39**, L15702, https://doi.org/10.1029/2012GL052483.

Zanchettin, D., S. W. Franks, P. Traverso, and M. Tomasino, 2008: On ENSO impacts on European wintertime rainfalls and their modulation by the NAO and the Pacific multi-decadal variability described through the PDO index. *Int. J. Climatol.*, **28**, 995–1006, https://doi.org/10.1002/joc.1601.